Received: 30 May 2023 | Revised: 12 March 2024 | Accepted: 25 March 2024

DOI: 10.1002/esp.5842

RESEARCH ARTICLE

ESPL WILEY

Improving predictions of critical shear stress in gravel bed rivers: Identifying the onset of sediment transport and quantifying sediment structure

Rebecca A. Hodge[1] | Hal E. Voepel[2] | Elowyn M. Yager[3] | Julian Leyland[2] | Joel P. L. Johnson[4] | David A. Sear[2] | Sharif Ahmed[5]

[1]Department of Geography, Durham University, Durham, UK

[2]Geography and Environmental Science, University of Southampton, Southampton, UK

[3]Center for Ecohydraulics Research, Department of Civil and Environmental Engineering, University of Idaho, Moscow, Idaho, USA

[4]Department of Geological Sciences, University of Texas at Austin, Austin, Texas, USA

[5]Diamond Light Source, Harwell Science and Innovation Campus, Didcot, Oxfordshire, UK

Correspondence
Rebecca A. Hodge, Department of Geography, Durham University, Durham, UK.
Email: rebecca.hodge@durham.ac.uk

Funding information
RAH, HEV, JL and DAS acknowledge funding from the Natural Environment Research Council, grant numbers NE/K012304/1 and NE/K013386/1. EY acknowledges funding from the US National Science Foundation, grant EAR1921790.

Abstract

Understanding when gravel moves in river beds is essential for a range of different applications but is still surprisingly hard to predict. Here we consider how our ability to predict critical shear stress (τ_c) is being improved by recent advances in two areas: (1) identifying the onset of bedload transport; and (2) quantifying grain-scale gravel bed structure. This paper addresses these areas through both an in-depth review and a comparison of new datasets of gravel structure collected using three different methods. We focus on advances in these two areas because of the need to understand how the conditions for sediment entrainment vary spatially and temporally, and because spatial and temporal changes in grain-scale structure are likely to be a major driver of changes in τ_c. We use data collected from a small gravel-bed stream using direct field-based measurements, terrestrial laser scanning (TLS) and computed tomography (CT) scanning, which is the first time that these methods have been directly compared. Using each method, we measure structure-relevant metrics including grain size distribution, grain protrusion and fine matrix content. We find that all three methods produce consistent measures of grain size, but that there is less agreement between measurements of grain protrusion and fine matrix content.

KEYWORDS
bedload transport, computed tomography scanning, critical shear stress, gravel bed rivers, terrestrial laser scanning

1 | INTRODUCTION AND AIM

In gravel-bed rivers, the river bed starts to be entrained when the applied shear stress (τ) is greater than the critical bed shear stress (τ_c) characterising the sediment surface. Predicting when sediment will move is essential for a wide range of management applications. For example, sediment erosion and deposition can change channel capacity, and hence the probability of flooding (Lane et al., 2007). The habitat quality and stability of restored rivers depend on whether the new channel bed is mobile under applied flows (Snyder et al., 2009). Similarly, engineered structures in rivers may need a level of protection that is tailored to likely sediment transport rates (Habersack et al., 2016). τ_c can also be a fundamental control on river channel geometry. The near-threshold model of channel geometry suggests that channels adjust their width and depth such that, at bankfull, τ is approximately equal to 1.2 τ_c (Phillips et al., 2022; Phillips & Jerolmack, 2019). Consequently, predictions of bankfull channel geometry using this model also require an accurate estimate of τ_c. Other laboratory and field studies suggest that τ and τ_c adjust such that the reach transport capacity is equal to the imposed upstream sediment supply (Dietrich et al., 1989; Madej et al., 2009; Pfeiffer et al., 2017), which still implies that τ_c indirectly influences channel geometry and slope.

Shields (1936) showed that in a bed of uniform-sized spherical grains, τ_c is proportional to grain diameter, such that dimensionless critical shear stress (τ^*_c; Shields' criterion) is constant across grain

sizes for the hydraulically rough flow in gravel bed rivers, where $\tau^*_c = \tau_c/g\,(\rho - \rho_s)\,D$ (D = grain size, ρ = density of water, ρ_s = density of sediment and g = acceleration due to gravity). Subsequently, a number of formulas have been produced that predict τ^*_c as a function of grain size or channel slope (e.g. Lamb et al., 2008; Perret et al., 2023). However, studies in conditions more representative of natural channels have shown that τ^*_c is far more variable than suggested by grain size or slope alone, with spatial and temporal variations caused by factors including grain packing, grain protrusion, flow history, the presence of cohesive fines, grain shape, bed slope, relative roughness and the grain size distribution (GSD) of the bed (e.g. Barzilai et al., 2012; Buffington et al., 1992; Buffington & Montgomery, 1997; Fenton & Abbott, 1977; Kirchner et al., 1990; Lamb et al., 2008; Laronne & Carson, 1976; Li & Komar, 1986; Masteller et al., 2019; Masteller & Finnegan, 2017; Ockelford & Haynes, 2013; Perret et al., 2023; Prancevic & Lamb, 2015; Recking, 2009; Reid et al., 1985; Schmeeckle et al., 2007; Warburton & Demir, 2000; Wiberg & Smith, 1987).

The combined influence of multiple controlling factors means that not only does τ^*_c vary spatially and temporally between rivers, but it can also be highly variable within an individual reach, such as spatial variation in τ^*_c between morphological units (Hodge et al., 2013; Sear, 2003). Consequently, despite the importance of τ^*_c, we still lack consistent, reliable methods to predict it. Phillips et al. (2022) report that, even after accounting for the impact of grain size on τ_c, values of τ_c cannot currently be predicted any better than to a factor of 10, leading them to conclude that for predicting channel geometry, 'the foremost challenge is to determine the appropriate entrainment threshold'. Although recent work has developed methods for predicting τ^*_c with reported lower uncertainties of 25% to 50% (Feehan et al., 2023; Perret et al., 2023), these approaches have not been widely applied. Consequently, for many applications, τ^*_c is still simply estimated to be a constant with a value somewhere between 0.03 and 0.06 (Buffington & Montgomery, 1997). However, this range equates to a doubling of the flow depth at which sediment will start to move, limiting the accuracy of any predictions derived from these values. To estimate τ^*_c from changing channel conditions, Johnson (2016) proposed that, instead of being assumed to be constant, τ^*_c should be treated as a state function which evolves in space and time depending on local bed characteristics and sediment transport rate. But, we do not currently know what form such functions should take.

Here we argue that improved predictions of τ_c require better understanding both of how the grain-scale structure of a sediment bed alters τ_c, and of the processes that cause the gravel-bed structure to change. We focus on sediment structure (including grain arrangement and the amount of cohesive fines around grains) because it has been widely demonstrated to affect τ_c (Charru et al., 2004; Cúñez et al., 2022; Fenton & Abbott, 1977; Galanis et al., 2022; Johnston et al., 1998; Kirchner et al., 1990; Voepel et al., 2019; Yager, Schmeeckle, & Badoux, 2018). Furthermore, structure can adjust rapidly within and between transport events, changing τ_c more quickly than changes in other factors such as grain size and shape, and providing a mechanism by which channel beds can rapidly adjust to changing flow and sediment supply conditions (e.g. Kirchner et al., 1990; Perret et al., 2020). If we understand how the grain-scale structure determines τ_c, then we can identify which properties of the bed we need to measure to predict τ_c at any given location as well as to predict variations in τ_c between different locations. Consequently, such data will also enable the development of new predictive relationships for τ_c.

The aim of this paper is to demonstrate how recent advances in field-based methods provide new opportunities to better understand the grain-scale controls on τ_c, through both a review of the literature and consideration of a new dataset. We focus primarily on field-based studies as we want to understand τ_c in these settings; we acknowledge the contributions made by laboratory and other approaches but do not provide a complete review of these methods. We focus on advances in two areas: (1) methods to identify the onset of bedload transport; and (2) methods to quantify grain-scale gravel bed structure. The first area is important because identifying the conditions under which sediment starts to move shows how much τ_c varies within and between rivers. Advances in the second area are required because the difficulty of measuring sediment structures means that we currently have very limited information on how they change spatially and temporally. We illustrate the range of methods that can be used to measure grain-scale sediment structure in the field by presenting the first direct comparison between three different methods: direct measurements of sediment properties, terrestrial laser scanning (TLS) data and computed tomography (CT) scanning data. We use the data from the three methods to calculate grain-scale properties, including grain size, protrusion, and contact with cohesive fines, and compare how the distributions of these properties vary between the different methods. We conclude by considering how recent methodological advances could be combined to identify which aspects of sediment structure most closely control values of τ_c, and hence which properties of gravel beds should be measured to understand how τ_c changes and to improve τ_c predictions.

2 | METHODS TO MEASURE τ_c

One common approach to quantifying τ_c in field settings is to identify the flow conditions at which sediment starts to move and to assume that the applied shear stress (τ) is equal to τ_c of the mobilised sediment. This approach requires concurrent measurements of sediment entrainment and the flow. We start with a brief overview of the methods used to measure and model flow, before discussing methods for measuring sediment entrainment. We split the latter into two categories: continuous bedload monitoring (both direct and indirect approaches) and methods for recording the movement of individual grains. In each case, we focus on recent advances and point the reader towards reviews of more established techniques.

2.1 | Measuring and modelling flow

The aim of flow measurements in this context is to estimate τ. Reach-averaged shear stress is often calculated by measuring flow stage within one or more surveyed cross-sections, and using the average depth from all cross-sections, water surface slope (or bed slope) and the assumption of uniform flow. Such an approach seems to be appropriate when sediment transport is also being measured in a reach-averaged way, or where the location of the mobile grains within the reach is unknown. However, unless the channel is unusually uniform,

τ and hence sediment transport are likely to be spatially variable, and so the reach-average shear stress will be an underestimate of the higher local shear stress in the areas of the bed where sediment first starts to move (Adams & Eaton, 2022; Ferguson, 2003; Lisle et al., 2000; Monsalve et al., 2016; Nelson et al., 2010; Segura & Pitlick, 2015). Conversely, the reach-averaged shear stress can be an overestimate of the local shear stress acting on sediment when part of the stress is borne by significant large roughness elements (e.g. woody debris, immobile boulders and vegetation) (Buffington & Montgomery, 1997; Lamb et al., 2008; Mueller et al., 2005; Nitsche et al., 2011; Schneider et al., 2015; Yager et al., 2007; Yager, Turowski, et al., 2012). A range of methods account for the effects of these large roughness elements or for the influence of relatively shallow flow on the onset of motion. These methods include stress partitioning or roughness partitioning equations that divide the bed and consequently the shear stress between roughness elements and sediment, and τ_c equations based on relative roughness effects. Even in uniform reaches without large roughness elements, the reach-averaged shear stress is still often a poor proxy for the fluctuating fluid forces acting on particles that actually cause sediment motion (Celik et al., 2013; Diplas et al., 2008; Nelson et al., 1995; Schmeeckle et al., 2007; Yager, Venditti, et al., 2018; Yang et al., 2016).

If the aim of data collection is to identify whether τ_c varies temporally in a particular channel (Masteller et al., 2019; Pretzlav et al., 2020), then overestimates or underestimates of local τ may be less important as long as the error in the estimate is consistent over time. However, if the aim is to use the value of τ_c estimated from measurements of τ to make predictions in other channels, then it is likely to be necessary to consider how channel morphology affects the relationship between average and local values of τ. Measurements of τ could be improved by 2D flow data (i.e. measurements in multiple locations across the channel) that estimate the spatial distribution of τ. For grains with a known location, this would provide a way of comparing their mobility to local τ (Smith et al., 2023). Even for bedload measurements that are not location specific, 2D flow data would enable analysis of the extent to which average τ represents local conditions when grains start to move. However, measuring τ spatially at the moment of grain entrainment is not straightforward in the field, relying on the deployment of flow monitoring equipment such as Acoustic Doppler Current Profilers (ADCP). These instruments are capable of measuring the vertical distribution of flow through the water column but rely on being deployed across multiple transects to build a 3D map of the spatial distribution of flow conditions, something that is time consuming and often not possible in small channels and steeper headwater systems. Furthermore, velocity cannot be measured in all locations simultaneously. New small Autonomous Surface Vehicles (ASVs) have facilitated systematic surveys using ADCP and related techniques (Tomsett & Leyland, 2019), although the surveys are still relatively time consuming as vessel speeds should ideally be limited to the same or less than the flow velocity being measured. In addition, ASVs typically have maximum speeds of around 6 knots, meaning that in very fast flowing water they simply cannot navigate against the flow. New field-based PIV (Particle Imaging Velocimetry) techniques might also provide an opportunity to quantify 2D flow patterns (Dobson et al., 2014; Eltner et al., 2021; Fujita et al., 1998), although there is still the need to convert from surface velocity patterns to bed τ, and they often only work during daylight. This means that modelling of the flow is likely the best approach to estimating bed τ (Monsalve et al., 2016; Segura & Pitlick, 2015), with some field data (water surface elevations and flow velocities) used for model calibration and validation.

2.2 | Continuous bedload monitoring techniques

One approach to measuring τ_c is to use continuous or frequent monitoring of bedload transport and to identify the times at which sediment starts to be entrained. Continuous or frequent measurements of bedload can be measured directly (e.g. using bedload samplers or bedload traps) or indirectly through measuring the sounds and vibrations produced by moving particles. In both cases, there can be uncertainty in defining the point at which sediment starts to move, reflecting the stochastic nature of bedload under low excess τ and measurement precision.

Direct measurements of bedload transport rates using bedload samplers (e.g. Emmett, 1980) or bedload traps (e.g. Reid et al., 1980) have been extensively used to determine τ_c. In this method, bedload fluxes are measured for a range of flow conditions and a reference dimensionless shear stress is calculated as the value of τ^* that causes a small but measurable dimensionless transport rate, which is called the reference transport rate (e.g. Perret et al., 2023). Approaches vary in the literature in terms of the method for nondimensionalizing the bedload transport rate and the assumed value of the reference transport rate. In addition to these methodological uncertainties, other potential uncertainties are driven by potential errors in bedload sampling, scatter in the bedload transport data, and curve fitting between dimensionless shear stress and dimensionless bedload transport rates. Such calculations can either occur for the entire GSD or for individual grain sizes, which enables calculation of a reference dimensionless shear stress for each grain size and a hiding function. The use of bedload samples and the reference shear stress approach have been discussed previously (Ancey, 2020; Buffington & Montgomery, 1997; Parker, 1990; Recking, 2010; Wilcock & Crowe, 2003) and are not further reviewed here.

Indirect techniques monitor sediment transport by recording the sounds and vibrations produced by moving bedload. Most long-term records use indirect monitoring approaches rather than direct ones (Habersack et al., 2017). Hydrophones and seismic monitoring record the energy released into the environment by bedload (Burtin et al., 2008; Geay et al., 2020; Gimbert et al., 2018; Hsu et al., 2011; Roth et al., 2014), whereas geophones, impact plates and pipes record the energy released when the grains interact with a specific monitoring device (Beylich & Laute, 2014; Hilldale et al., 2015; Rickenmann et al., 2012). Such approaches have potential to provide information on bedload transport rates and grain sizes, but our focus here is on when bedload transport starts and stops. Seismic and hydrophone techniques can record bedload motion across a larger area than direct samplers and impact plates, and so are more likely to identify the onset of transport.

Multi-year bedload transport data from both direct and indirect methods has been used to identify how τ_c varies over time. Reid et al. (1985) first used continuous bedload trap data to show that τ_c was higher following long periods of low flows which consolidated the bed, and lower when sequential floods loosened the bed. Using

impact plate data, Turowski et al. (2011) found that, in three proglacial streams, the discharge at which sediment started to move was correlated with the discharge at which sediment stopped moving in the previous flood event, indicating the impact of flow history on τ_c. Rickenmann (2018) attributed these changes to rearrangements in bed structure. Turowski et al. (2011) found that the pattern was less clear in the Erlenbach, Switzerland, a channel in which sediment transport is dominated by summer rain-driven events. Further work by Masteller et al. (2019) in the Erlenbach suggested that larger antecedent flow magnitudes increases subsequent values of τ_c, but only up to a certain antecedent flow threshold. Above this threshold, τ_c was either independent of the antecedent flow magnitude or possibly decreased with greater flows. These temporal variations in τ_c are interpreted as reflecting changes in bed structure, but concurrent measurements of bed structure were not collected. At the same location, Rickenmann (2020) found that τ_c varied inversely with a disequilibrium ratio (observed bedload divided by transport capacity), and hypothesised that this reflected the impact of sediment supply on sediment structure. Increased sediment supply results in a thicker active layer and looser packing, hence reduced τ_c and increased bedload transport; during periods with reduced sediment supply, the bed is stabilised, increasing τ_c and reducing bedload transport. Other long-term geophone records have not been directly analysed to identify temporal variations in τ_c, although Aigner et al. (2017) show differences in transport rates before and after a bedload pulse, and Downs and Soar (2021) identified the importance of flow history and sediment supply factors on transport rates. Installing these instruments requires a large amount of in-channel infrastructure, prohibiting easy application of these techniques to a wider range of rivers.

Seismic signals recorded adjacent to a river have also been shown to correlate with bedload transport. Early evidence for this correlation was hysteresis between the seismic signal at certain frequencies and measured discharge, enabling identification of the discharge at which sediment started to move (Govi et al., 1993; Hsu et al., 2011). There has been a recent rapid growth of data and theory in this area (Anthony et al., 2018; Bakker et al., 2020; Barrière et al., 2015; Chao et al., 2015; Cook et al., 2018; Gimbert et al., 2014; Lagarde et al., 2021; Misset et al., 2020; Polvi, 2021; Roth et al., 2014; Schmandt et al., 2013, 2017; Tsai et al., 2012), which has demonstrated that seismic data can provide robust predictions of relative sediment flux, enabling the onset of sediment transport to be identified. However, measuring bedload transport rates is harder because of the multiple factors that contribute to the seismic noise that is produced and the need to differentiate between the noise of the bedload, the turbulent flow and other environmental signals (Cook & Dietze, 2022). Seismic approaches provide new opportunities for continuous monitoring, with the lack of in-channel infrastructure meaning that seismometers can be easily installed in a variety of locations, including those where in-stream infrastructure may be destroyed by extreme events. However, as far as we know, this technique has not yet been used to analyse variations in τ_c.

2.3 | Monitoring individual grains

An alternative approach to measuring τ_c is to track the transport of individual tracer grains through space and time, from which their time of entrainment can be related to hydraulic parameters. The methods used to do this range from simple tagging of grains to enable them to be manually relocated following a flow event, through to continuous monitoring of the accelerations experienced by the grain.

The simplest method of tagging grains with spray paint, magnets, or passive or active RFID tags, and mapping their locations before and after sediment transport events have been widely applied (e.g. Bradley & Tucker, 2013; Ferguson et al., 1996, 2002, 2017; Ferguson & Hoey, 2002; Goode & Wohl, 2010; Haschenburger, 2013; Hodge et al., 2011; Lenzi et al., 2006; Liébault et al., 2024; MacVicar & Roy, 2011; Mao et al., 2008; Oldmeadow & Church, 2006; Scheingross et al., 2013; Yager, Dietrich, et al., 2012). If tracer particles move during an event, then estimation of τ_c requires assumptions about the flow within the hydrograph that was responsible for transport of a given particle size. The maximum (commonly called the competence approach) and 84th percentile of the mobile tracer distribution have been assumed to represent the grain size that would just begin transport at peak τ within a hydrograph (Lenzi et al., 2006; Mao et al., 2008; Scheingross et al., 2013; Yager, Dietrich, et al., 2012). An alternative approach is to only use the tracer particle sizes that move a short distance (e.g. less than one diameter or less than 1 m) from installation (Lenzi et al., 2006; Mao et al., 2008; Scheingross et al., 2013). By combining tracer transport data from multiple floods, τ_c for a range of bed grain sizes and hiding functions can be estimated (Lenzi et al., 2006; Mao et al., 2008; Yager, Turowski, et al., 2012). This approach also enables estimation of τ_c for individual sediment patches on the bed or for different areas of the bed (MacVicar & Roy, 2011; Scheingross et al., 2013; Smith et al., 2023; Yager, Dietrich, et al., 2012). Given all of the assumptions that are made in identifying the flow that moved tracers and in the representative tracer size or distance travelled, considerable uncertainties remain in using tracers to estimate τ_c.

Statistical approaches have the potential to extend information that can be extracted from bedload tracers (MacVicar & Papangelakis, 2022), but these data still cannot generally identify the timing of grain entrainment and resting periods during a flow event. Alternatively, antennas can be installed across the river bed to record the timing of overpassing RFID-tagged grains. Such data provide starting times of sediment transport (Casserly et al., 2021), but only for grains that cross the antenna following entrainment. The use of active RFID tags means that the antennas can be outside the channel, such as on a bank (Cassel et al., 2021) or attached to a drone (Cassel et al., 2020), and repeat drone surveys during a flow event may be able to identify the timing of individual grain displacements. Ergenzinger et al. (1989) and Habersack (2001) were among the first to use radio transmitter tagged stones as a Lagrangian method of simultaneously tracking grain entrainment timing, jump distances and resting periods during a flood event, and such data from a number of grains could be a valuable way of evaluating spatial and temporal differences in τ_c. Sear et al. (2002) show that data from logging pebbles that record the strength of an electromagnetic field produced by buried wire loops can be used to track changes in pebble location in the littoral zone. However, tracking techniques are still not commonly applied in fluvial bedload research, despite ongoing developments in electronics and tracking methods in other fields (Dini et al., 2021; Hart & Martinez, 2022; Noonan

et al., 2015). Although challenging, developing these techniques to link grain positions and entrainment/rest times throughout flood events would be an exciting new area for development, although the same challenges of linking the motion of the tracer particle to the local fluid forces remain.

Accelerometers and related sensors embedded in tracer clasts hold great potential to measure grain orientations, the timing of movements and potentially even net forces acting on grains (Maniatis, 2021; Olinde & Johnson, 2015; Pretzlav et al., 2020, 2021). Such data enable τ_c to be estimated from concurrent measurements of flow and distributions of the timing of movements. Pretzlav et al. (2020) measured 15 578 individual grain movements of 21 tracers over ~30 days of diurnal snowmelt discharge and found systematic τ_c changes over time which correlated with both cumulative discharge and also changes in discharge from one day to the next. One limiting factor of such data to date is that locations of instrumented grains within the channel during transporting floods are unknown, and so entrainment can only be linked to reach-averaged conditions, not local flow conditions. Another potential issue is that the minimum tracer size is limited by the size of the electronics and especially batteries, with larger batteries increasing the duration of data collection. Consequently, the instrumented grains may not be representative of most grains in the channel, although the size of hardware is decreasing over time. Tracers used by Olinde and Johnson (2015) and Pretzlav et al. (2020) approximated reach D_{84} and D_{50}, respectively (where D_{50} and D_{84} are the 50th and 84th percentiles of the GSD). Technological advances such as controlling when grains do or do not record data may also increase battery life and memory. Wireless data streaming would enable data to be obtained in real time and to not be dependent on subsequent grain recovery, although the need to transmit signals through water rather than air makes this harder to achieve (Biggs et al., 2022).

3 | METHODS TO MEASURE SEDIMENT STRUCTURE

Sediment structure has been widely demonstrated to affect τ_c. But measuring the 3D structure of gravel beds is not straightforward as opaque grains mean that everything below the surface is hidden from view. Here we consider three different approaches to quantifying sediment structure in the field, presented in increasing order of surface representation. The first approach is not to measure structure directly but rather the impact of the structure by measuring the forces required to displace individual grains. These data can be combined with other direct measurements, such as 1D measurements of grain exposure. The second approach is using survey techniques such as TLS or structure from motion (SfM) photogrammetry, which measure the surface topography of the bed. The final approach is measuring 3D grain topography using CT or magnetic resonance imaging (MRI) scanning, which provides an image of the entire 3D structure of the bed surface and the internal bed structure. For each of these approaches, there is the additional complexity of knowing which metrics to measure in order to best estimate τ_c of the bed. We start with an overview of the range of metrics that have been developed to describe sediment structure before considering how each method has been applied.

3.1 | Selecting metrics

Previous work to identify metrics that relate to τ_c has been motivated by the parameters included in the grain-scale entrainment models of Kirchner et al. (1990), Voepel et al. (2019), Wiberg and Smith (1987) and Yager, Schmeeckle, and Badoux (2018), which include grain protrusion (which is sometimes separated into projection and exposure), pivot angle, the volume of sediment overlying the moving grain, the presence of cohesive sediment around the grain, and the bulk sediment friction angle. Bulk sediment friction angle or the intergranular friction angle is in turn controlled by a large number of interacting variables such as the solid volume fraction (inverse of porosity), particle orientation, imbrication, shape and angularity. At the particle scale, intergranular friction is mechanistically controlled by force chains, which are in turn influenced by the stress history of the bed (Booth et al., 2014; Charru et al., 2004; Cúñez et al., 2022; Galanis et al., 2022). Grain shape, grain packing density, particle clusters and surface roughness have also been hypothesised to affect τ_c through their impacts on both bed structural parameters and the applied fluid forces (Buxton et al., 2015; Curran & Tan, 2014; Curran & Waters, 2014; Deal et al., 2023; Hassan & Reid, 1990; Marquis & Roy, 2012; Oldmeadow & Church, 2006; Perret et al., 2020; Wittenberg & Newson, 2005). Furthermore, cluster impacts will change within and between flood events because of variations in the spatial density and form of clusters and other grain arrangements.

None of the simple force balance entrainment models such as Kirchner et al. (1990) have been fully validated because of the difficulty of measuring both grain-scale parameters and τ_c for the same patch of sediment. However, they have been tested in other ways. Yager, Schmeeckle, and Badoux (2018) showed that their resisting force model could reproduce measured distributions of resisting forces using measured values of protrusion and plausible distributions of pivot and intergranular angles. Hodge et al. (2013) parameterised the model of Kirchner et al. (1990) using field measurements and produced plausible values of τ_c and showed that they varied spatially through a riffle–pool sequence. Smith et al. (2023) showed that measured patch-scale hiding functions can be partly explained by patch-scale protrusion variations. Hodge et al. (2020) showed that their distribution of τ_c modelled using the 3D entrainment model of Voepel et al. (2019) was consistent with predictions from bedload transport models. The work of Yager, Schmeeckle, and Badoux (2018) and Hodge et al. (2020) using these models and field or flume data has suggested that grain protrusion is the parameter that best correlates with τ_c values. This is also supported by work such as the pioneering lab experiments of Fenton and Abbott (1977) in which grain protrusion was inversely correlated with entrainment force. For each of the different methods, we consider which metrics can be measured, with a particular focus on those used as parameters in force (or moment) balance entrainment models.

3.2 | Direct measurements

Sediment structure can be assessed indirectly by measuring the maximum force required to dislodge a grain from a river bed, as first applied by Johnston et al. (1998). In this approach, individual grains are selected and a force gauge is used to apply a horizontal force to

the centre of the upstream exposed face of each grain until the grain is moved from its pocket by a grain diameter. Other applications have stuck loops to grains and measured the maximum vertical force instead of, or alongside, horizontal force measurements (Hodge et al., 2013; Sanguinito & Johnson, 2012). Applications of force gauge measurements have included assessing: differences in sediment structure through a riffle–pool sequence (Hodge et al., 2013), the influence of bed slope and jamming ratio on the mobility of large grains in steep channels (Prancevic & Lamb, 2015), differences in mobility between different grain sizes (Johnston et al., 1998), effects of salmon spawning on particle mobility (Buxton et al., 2015), and the impact of overlying grains on mobility (Sanguinito & Johnson, 2012). The need to access the bed means that these measurements can only be collected from exposed bars or dry channels.

Dislodgement forces can be contextualised by measuring additional metrics in the field. Grain size and weight are normally measured, as normalising dislodgement force by grain weight reveals the additional contribution of sediment structure to the grain's resistance to motion. This normalised force has sometimes been converted into a pivot angle (Johnston et al., 1998). This conversion may have been motivated by previous tilt-table experiments, in which grains were placed onto glued or cast sediment surfaces, and the pivot angle was the tilt at which the grain was displaced from its location and reflects the grain's pocket geometry (Buffington et al., 1992; Kirchner et al., 1990; Li & Komar, 1986). However, pivot angles calculated from forces measured in the field are unlikely to be a direct representation of the grain's pocket geometry, as the measured force also depends on factors that are not included in tilt-table experiments, for example, displacement of overlying and/or downstream grains, friction between the particle and any surrounding/burying sediment, and the presence of cohesive fine sediment (Hodge et al., 2020; Yager, Schmeeckle, & Badoux, 2018).

Other metrics that have been collected alongside dislodgement forces include the amount of grain area covered by overlying grains (Sanguinito & Johnson, 2012), and channel width and slope (Prancevic & Lamb, 2015). Despite being easy to measure with a ruler, grain protrusion has not been commonly measured directly in the field. Yager, Schmeeckle and Badoux (2018) present the only published data of which we are aware that directly compare grain protrusion to both measured dislodgment force and to empirical field τ^*_c. They find that both dislodgement force normalised by grain weight and empirical field τ^*_c decreases as protrusion increases, providing strong evidence that suggests protrusion is a first-order control on grain entrainment and an important metric to measure.

3.3 | Surface topography

High-resolution survey techniques such as TLS and SfM photogrammetry have been used to measure surface topography of gravel beds in the field (Bertin & Friedrich, 2016; Butler et al., 1998; Heritage & Milan, 2009; Hodge et al., 2009; Smart et al., 2004). As with direct measurements, TLS and SfM photogrammetry data are typically only collected from exposed areas of the channel. However, topographic data can also be collected using SfM photogrammetry through or under water (Carrivick & Smith, 2019; Kalacska et al., 2018), TLS through water under certain conditions (Smith et al., 2012), or using increasingly high-resolution shallow-water survey techniques (Tomsett & Leyland, 2019), opening up these methods to a wider range of channels, although data quality may not be as high as with sub-aerial methods. Sediment structure can be inferred from the point clouds or DEMs in two different ways: methods that quantify the average or bulk properties of the sediment bed, and methods that segment out individual grains and calculate their properties. Some of these approaches use the 3D point clouds of the gravel surfaces, whereas others interpolate the data into 2.5D DEMs in which each location across the bed has a single elevation.

The most commonly calculated bulk metric is the standard deviation of elevations (σ_z), which is a measure of surface roughness (Smart et al., 2004). For grains of a given size, changes in packing have potential to affect σ_z. However, laboratory experiments measuring the impact of water working and imbrication on σ_z suggest that the direction and magnitude of any changes will depend on grain size and shape, and are not straightforward to predict (Masteller & Finnegan, 2017; Ockelford & Haynes, 2013; Pearson et al., 2017). σ_z also strongly depends on grain size, with σ_z increasing with increasing D_{50} or D_{84} (Pearson et al., 2017; Rychkov et al., 2012; Vázquez-Tarrío et al., 2017; Woodget & Austrums, 2017). Consequently, sediment structure cannot be quantified using σ_z without independent grain size data with which to normalise σ_z. Semi-variograms have also been used to measure surface roughness at different scales, and results have been interpreted to identify length scales of grain clustering (Butler et al., 2001; Curran & Waters, 2014; Ockelford & Haynes, 2013; Robert, 1988); however, the scale breaks in the semi-variogram can be ambiguous. Overall, there has only been limited work on identifying which bulk metrics best represent grain mobility and hence might be used to predict τ_c (e.g. Perret et al., 2020). Coarse grain clustering can also be quantified objectively, and clustering statistics correlate with bed stability (Hassan, Saletti, Zhang, et al., 2020; Johnson, 2017).

Protrusion can be measured for individual grains in a DEM as the difference between the maximum elevation of the grain and the mean elevation of the surrounding area (Hodge et al., 2013), but this requires the outline of each grain to be identified. Outlines can be digitised manually, although this is time consuming, potentially limiting sample size. Different methods have been developed for automatic grain edge detection in images of gravel beds, in order to extract grain size information (Detert & Weitbrecht, 2012; Graham et al., 2005; Purinton & Bookhagen, 2019), but methods for automatic grain edge detection in topographic data have only been developed more recently (Steer et al., 2022; Wu et al., 2021). Such methods have potential to enable protrusion measurements to be automated across large TLS or SfM photogrammetry datasets, which could provide new insights into gravel bed mobility. For example, Yager et al. (2024) explore how automatic edge detection in topographic data can be combined with automated protrusion measurements to obtain protrusion and τ_c distributions for beds. However, we do not have robust criteria to define exactly how protrusion should be measured in terms of the distance over which the mean bed elevation should be calculated and whether protrusion needs to be calculated using the 3D grain topography or can be simplified into a 1D metric. Another possible approach to quantifying protrusion from DEMs is to identify local topographic maxima above a certain threshold in the DEM. In an analysis of flume bed DEMs, Masteller and Finnegan (2017) assumed that these maxima indicated grains with the highest protrusion, and found that subsequent bedload transport rates were enhanced when beds

had a higher number of these maxima, further supporting the importance of grain protrusion for entrainment.

3.4 | 3D scanning

The most complete method of measuring the structure of a gravel bed is to produce a 3D image of undisturbed bed samples using techniques such as CT or MRI scanning. Example applications include measuring porosity and fine sediment infiltration into gravel beds (Haynes et al., 2009; Kleinhans et al., 2008), and measuring the 3D structure of water-worked gravel beds (Hodge et al., 2020; Voepel et al., 2019). However, the applicability of such methods is limited by factors including: the maximum sample size that can be measured, which depends on the scan chamber size, sample density, beam strength and characteristics of the scanner; the need to extract and transport undisturbed samples from the field location to the scanner; and the incompatibility of MRI and magnetic objects (including magnetic minerals in sediment grains).

A further complication is that once 3D data have been collected, there is not an established way to measure relevant entrainment metrics in 3D. Possibly, the most thorough example is Voepel et al. (2019), who applied new methods to CT data at sub-millimetre resolution produced by scanning 0.25-m diameter baskets of water-worked gravel extracted from flume experiments. They developed image processing methods to segment out individual grains from the surrounding fine-grain matrix, and then for each grain, extracted physical characteristics including centre of mass, volume, surface area, maximum grain elevation, 3D axis lengths and orientations, and all grain-to-grain contact point locations. For each grain, a new simple 3D vector-based moment balance was used to calculate a τ_c value corresponding to every possible axis of rotation, where each rotation axis was formed by a viable contact pair. The smallest calculated value was retained as τ_c, and other entrainment metrics were calculated, including the grain's pivot, tilt and bearing angles at entrainment. The 3D model included a component of resistive, cohesive force because of contact with the fine-grain matrix, which was estimated using a model developed from lab experiments (see Voepel et al. [2019] for details). Modelled results showed that τ_c has a low correlation with pivot angle, whereas the strongest correlation was with grain protrusion (Hodge et al., 2020), supporting the findings of Yager, Schmeeckle and Badoux (2018). One area for future development is to improve the representation of interactions between the flow and bed structure in the entrainment model, as it currently assumes a uniform logarithmic flow profile across the bed surface.

The 3D scanning methods are being increasingly used in geoscience research (Lev & Boyce, 2020) and may provide an opportunity for coupled measurement of 3D sediment structure and τ, which could be used for testing models of τ_c. For example, Lakshmanan et al. (2014) placed an MRI-compatible flume within the scanner, in which they used a flow tracer to measure tracer dispersal into the gravel framework. If such a flume could be made large enough that forces would be sufficient to entrain sediment grains, and coupled with imaging techniques to measure spatial patterns of sediment and flow velocity (Amon et al., 2017; Coussot, 2020; Penn et al., 2017; Sederman et al., 2004), then both sediment structure and flow could be quantified throughout a grain entrainment event.

4 | COMPARISON OF DIFFERENT METHODS AT BURY GREEN BROOK

To test how well the three different approaches describe variations in sediment structure, we present data from the same river bed collected using all three methods: direct measurements, TLS and CT scanning. The field site, Bury Green Brook (near Bishop's Stortford, UK, 51.8486, 0.0807), is a small, gravel-bed, intermittently flowing channel, with a riffle–pool morphology. Bankfull channel width varies from 2.8 to 6.5 m, mean bankfull depth is 1.3 m, mean slope is 0.008, and D_{50} and D_{84} are between 27 and 42 mm, and 37 and 60 mm, respectively (Hodge et al., 2013). Previous direct measurements and topographic data from this site found a spatial variation in grain diameter, entrainment forces, and exposure between the pools, pool tails and riffles (Hodge et al., 2013). The new field data presented here were collected in April 2017, during zero flow conditions when the bed was fully exposed. We identified two riffle-pool sequences (Figure 1), each of which was visually sub-divided into riffle (R), pool head (H), pool deep (D) and pool tail (T) units. The upstream sequence starts at a pool head, and the downstream sequence at a pool deep. A ~1-m^2 patch was located within each unit, giving eight patches in total from which data were collected. The patches are labelled according to the unit that they are located in, with R1/H1/D1/T1 comprising the upstream sequence and D2/T2/R2/H2 being downstream. The three methods were all applied to each of the eight patches.

The year before these measurements was relatively dry compared to previous years (Figure 2), annual maximum flow at the River Ash Mardock gauging station 4.5 km downstream was 1.07 m^3 s^{-1} in the 2017 water year compared to 6.67 m^3 s^{-1} in the 2016 water year, with 2017 ranking 73rd out of the 80 years with annual maximum flow data (National River Flow Archive, 2023). Consequently, the field site is unlikely to have been water worked for several months prior to data collection. There was also evidence that people had accessed parts of the channel, potentially disturbing the bed. The data therefore are probably not representative of bed structure under normal water-worked conditions, and so cannot be used to infer spatial variations in morphological processes. Instead, we use these results to test whether the three different methods give similar values for the structural properties of the patches.

4.1 | Methods

4.1.1 | Direct measurements

Sediment structure within each patch was assessed by measuring the forces required to dislodge grains from the bed. Data were collected from ~50 grains from each patch. For half of the grains, we measured the maximum horizontal force (F_{push}) needed to move the grain by a grain diameter by applying a force in the streamwise direction using a handheld MecMesin Basic Force Gauge (200 N model). For the other grains, we measured the maximum vertical force (F_{pull}) needed to lift the grain from the bed using a loop of string glued onto the grain and attached to the force gauge. Grains were measured from downstream to upstream locations to avoid disturbing unmeasured grains. For each grain, we also measured the three axes ($D_a/D_b/D_c$), the upstream protrusion height (p_{direct}) with a ruler, which axis was

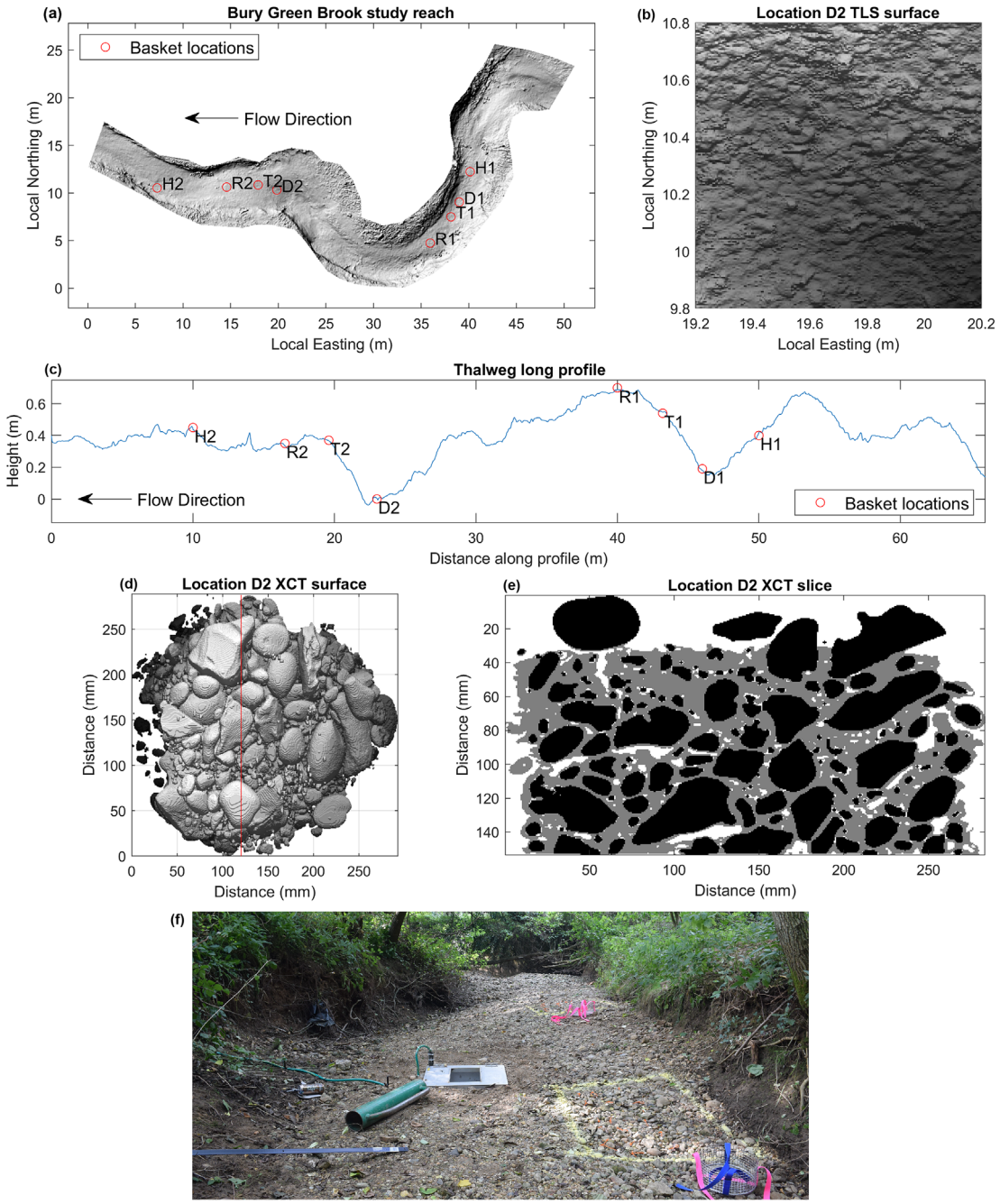

FIGURE 1 Bury Green Brook study reach. (a and c) Topography and long profile along centre of reach showing basket locations (note that not all patches are in the centre of the channel). (b) Terrestrial laser scan data from patch D2. (d and e) CT scan data from patch D2. (d) The top surface of the basket. (e) A cross-section through the basket along the red line in Figure 1d (looking towards $x = 0$). Grains are shown in black and fine-grained matrix in grey. (f) Photo of reach looking downstream from approximately location T2. [Color figure can be viewed at wileyonlinelibrary.com]

vertical prior to movement (which has length D_{vert}), and whether the pocket exposed by removing the grain contained fine-grained matrix. The latter measurement is included because this stream bed can contain a cohesive clay-based matrix which increases entrainment forces (Hodge et al., 2013). For each patch, we calculated the proportion of grains for which fine-grained matrix was observed, M_{prop}. In the analysis for each patch, we combine the data from all ~50 grains, with the exception of F_{push} and F_{pull} which were each measured for approximately half the grains. Because of field equipment failure, we do not have weights (W) for all grains. We instead predict the mass of these grains (M_{pred}) as a function of their three axes lengths using a relationship derived from the 178 grains for which masses were recorded. This relationship had a correlation coefficient of 0.96:

$$\log(M_{pred}) = -0.15049 + 0.929 \log(4\pi\rho_s D_a D_b D_c/6). \quad (1)$$

4.1.2 | TLS methods

TLS data were collected in April 2017 immediately prior to the force measurements and used multiple scan positions so that the entire channel bed was covered at a sub-centimetre point spacing (Figure 1). The mean absolute registration error was 3 mm. The TLS point cloud was cropped to the 1 m^2 area of each patch, and vegetation and other erroneous points were removed manually. Following Hodge et al. (2013), patches were detrended by fitting and subtracting a second-

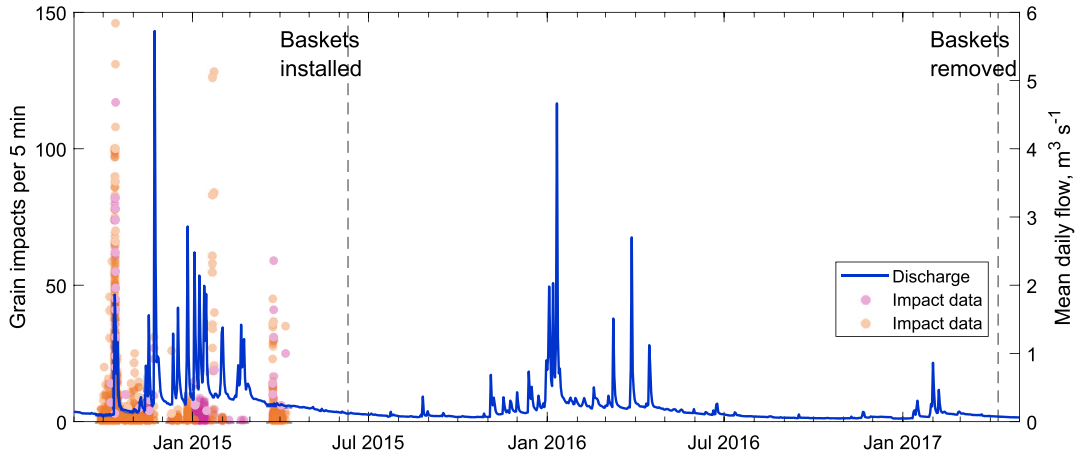

FIGURE 2 Discharge data from the River Ash Mardock gauging station 4.5 km downstream of the study location (National River Flow Archive, 2023) and bedload impact plate data from two sensors at the study location. Impact plate data are only available from the period prior to basket installation. However, they show that the flows during the first winter after installation were likely to be sufficient to waterwork the basket sediment. [Color figure can be viewed at wileyonlinelibrary.com]

order polynomial surface. Following Aberle and Smart (2003), surface roughness was calculated using the standard deviation of elevations (σ_z).

Grain size and grain protrusion were also estimated from the point clouds by applying G3Point (Steer et al., 2022) and Pro+ (Yager et al., 2024), respectively, to the central 0.3 × 0.3 m of each detrended point cloud. Details on G3Point are provided in Steer et al. (2022), and input parameter values were selected as those that minimised the difference between the GSD measured in the field and using G3Point. The reduced patch area was used to limit processing time and is the area of the bed over the CT basket. Between 11 and 45 grains were identified in each patch. Pro+ first determines grain perimeters from the point clouds of each grain identified by G3Point and then determines the area immediately surrounding every particle by conducting a search of a specified distance from the grain perimeter. Pro+ uses two measures of protrusion: p_{50}, which is the difference in elevation between the maximum elevation of the grain and the median surrounding bed elevation, and p_{10} which is protrusion relative to the 10th percentile of surrounding bed elevations (motivation for use of these percentiles is provided in Yager et al. (2024)).

4.1.3 | CT methods

To collect samples from Bury Green Brook for CT scanning, 0.25 m diameter wire baskets were levelled and buried in the centre of each of the eight patches in June 2015 (Figure 1), with the rim of each basket at a depth equivalent to 1.5 D_{50} below the surface of the bed so that the surface grains would be water worked by channel flows. During installation, the baskets were filled with the sediment excavated from the holes. Twenty-two months later in April 2017, the basket locations were resurveyed. The winter of 2016–2017 prior to excavation was dry, but during the first winter after installation (2015–2016), discharges recorded at the River Ash Mardock gauging station 4.5 km downstream were comparable to those associated with bedload mobilising events at the study location in the winter of 2014–2015 (Figure 2). We therefore assume that the bed was water worked after basket installation, and so there was no difference in the structure of the basket sediment and the surrounding bed. Any consequent disturbance of the bed during the low flow conditions would be expected to have occurred equally across the baskets and surrounding areas.

We first collected force measurements from the areas surrounding the baskets, taking care not to disturb the bed area within the basket. The baskets were then excavated and dipped in molten wax to stabilise the sediment within them. The baskets were CT scanned in the micro-focus Nikon Metrology µCT scanner at the µ-VIS X-Ray Imaging Centre, University of Southampton, UK. Each CT scan was scanned and processed following the procedure in Voepel et al. (2019). The 3D image was classified into sediment grains, areas of fine-grained matrix, and areas of air and wax. The following metrics were then measured for each sediment grain in the basket: axes length, volume, protrusion (p_{CT}), pivot angle and the proportion of the entire grain surface that is in contact with the fine-grained matrix (M_{areaCT}). Protrusion was measured as the vertical distance between the maximum elevation of the grain and the average surrounding bed elevation. For each grain, the latter was calculated over a distance D_{84} upstream and downstream of the 3D bounding box around the grain, where D_{84} was an average value from the entire reach. If this area fell outside the basket area, then basket surface was extended by tiling duplicate copies of the surface in areas where elevation data was absent. τ_c and τ^*_c were then predicted for surface grains using a 3D vector-based moment balance model (Voepel et al., 2019). Unless stated otherwise, results from the CT baskets are reported only for grains where it was possible to model a shear stress that was sufficient for entrainment (i.e. the grain could move without dislodging other grains), which is 12 to 57 grains per basket. This produces a sample of surface grains that is similar to the population of grains measured using the other techniques. The only exception was M_{areaCT}, which was also measured for all grains in the basket (M_{areaCT_all}, n = 741 to 2683 grains).

4.1.4 | Data analysis

We compare our data using two complementary approaches. The first approach is to compare the distributions of metrics between the eight different patches. For metrics that have been measured using only a single method, we use the Kruskal–Wallis test to identify significant differences between the patches ($\alpha = 0.05$). For metrics that have been measured using two or more methods (i.e. grain size, protrusion and matrix area), we perform a two-way comparison using the Scheirer–Ray–Hare test (with $\alpha = 0.05$) (Sokal & Rohlf, 1995). For all tests, we then use Dunn's post-hoc test (Dunn, 1964) to identify differences between patches and between methods where applicable. (This post hoc test is used to test for differences by patch or by method, but not both at once.) In Figures 3–6, groups that share an alphabetical label are not significantly different ($\alpha = 0.05$). We use non-parametric tests because the Levene's test (Levene, 1960) showed that for most metrics the variance between the eight patches was significantly different. For the categorical grain orientation data, we use the Chi-square to evaluate differences in distributions between patches.

The second approach is a cross-correlation analysis with the Pearson's test applied to 15 metrics. Each metric has eight data points, one from each patch. From direct measurements we use D_b and p_{direct}/D_b for all grains, F_{pull}/W, F_{push}/W and M_{prop}; from TLS data, we use σ_z, D_b, p_{50}/D_b and p_{10}/D_b; and from CT data, we use D_b, p_{CT}/D_b, τ_c, τ^*_c, M_{areaCT} and M_{areaCT_all}. Where we have a distribution of data from each patch, we use the median value. This analysis tests whether the data show expected correlations between different metrics, as identified by previous work (Hodge et al., 2013; Kirchner et al., 1990; Yager, Schmeeckle, & Badoux, 2018).

4.2 | Results

4.2.1 | Impact of past flow conditions

Unlike previous data (Hodge et al., 2013; Sear, 1996), these results do not show such a marked difference between grain properties in different morphological units (statistical results are provided in the following sections). For some properties, such as grain size, the difference between patches from the same unit is greater than the difference between patches from other units in the same riffle–pool sequence (Figure 3a). We hypothesise that the lack of differentiation between patch types reflects the lack of recent water-working flows. We therefore suggest that these patches are unlikely to be representative of riffle–pool sequences more generally. Our focus in this paper is instead on comparison of the three methods.

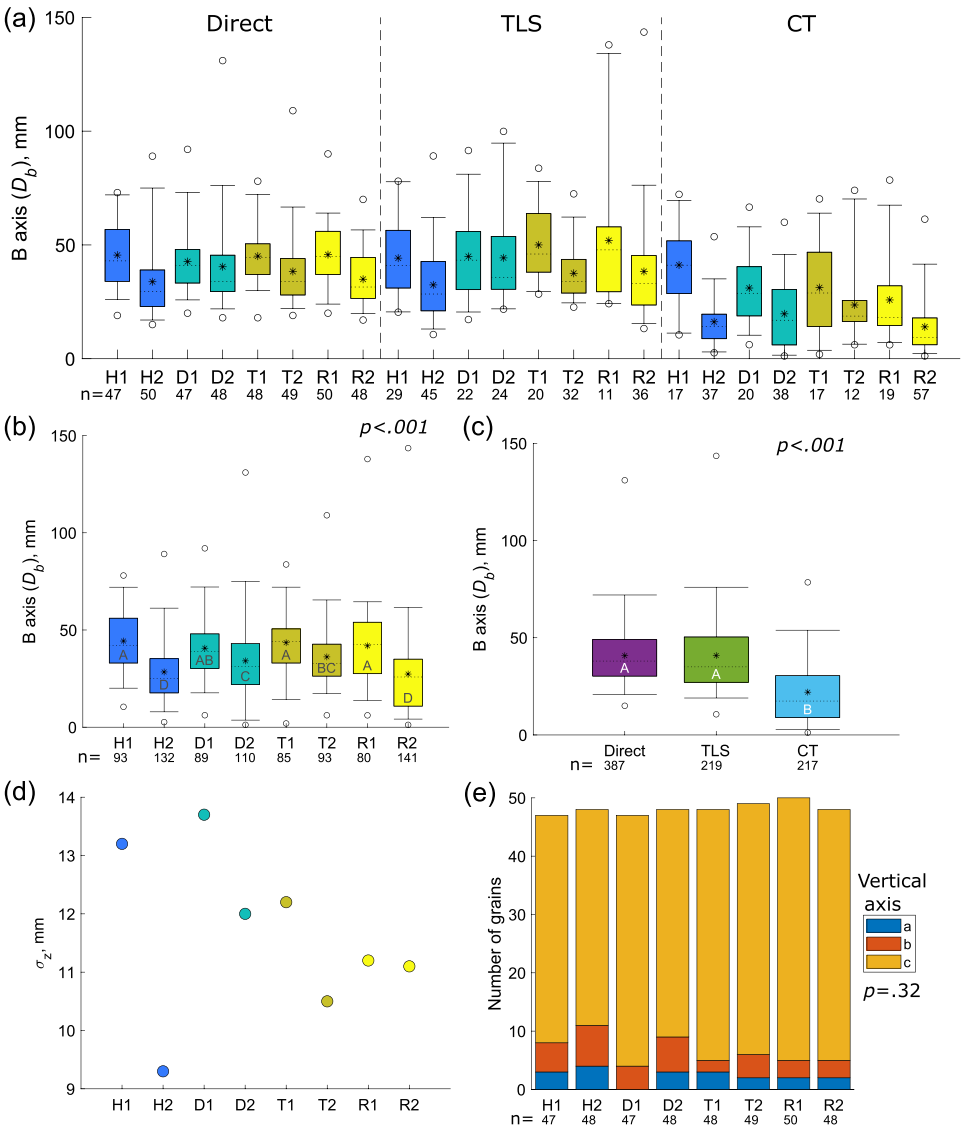

FIGURE 3 Grain size measurements. (a) *b*-axis (D_b) measured using all three methods; (b) the same data grouped by patch; (c) the same data grouped by method; (d) standard deviation of elevations (σ_z) calculated from the detrended Terrestrial Laser Scanning data of each patch; and (e) grain vertical axis. In all panels H: pool head; D: pool deep; T: pool tail; and R: riffle. 1 are the upstream patches, and 2 are the downstream patches. Boxplots show 25th to 75th percentiles, dashed line is the median, whiskers show 5th and 95th percentiles, open circles show min and max, and star is the mean. *n* indicates number of grains in each distribution. The Scheirer–Ray–Hare test shows significant differences between patches and between methods. In (b) and (c), groups sharing a capital letter are not significantly different as identified by post-hoc Dunn test. Differences between distributions in (e) are evaluated using a Chi-square test. [Color figure can be viewed at wileyonlinelibrary.com]

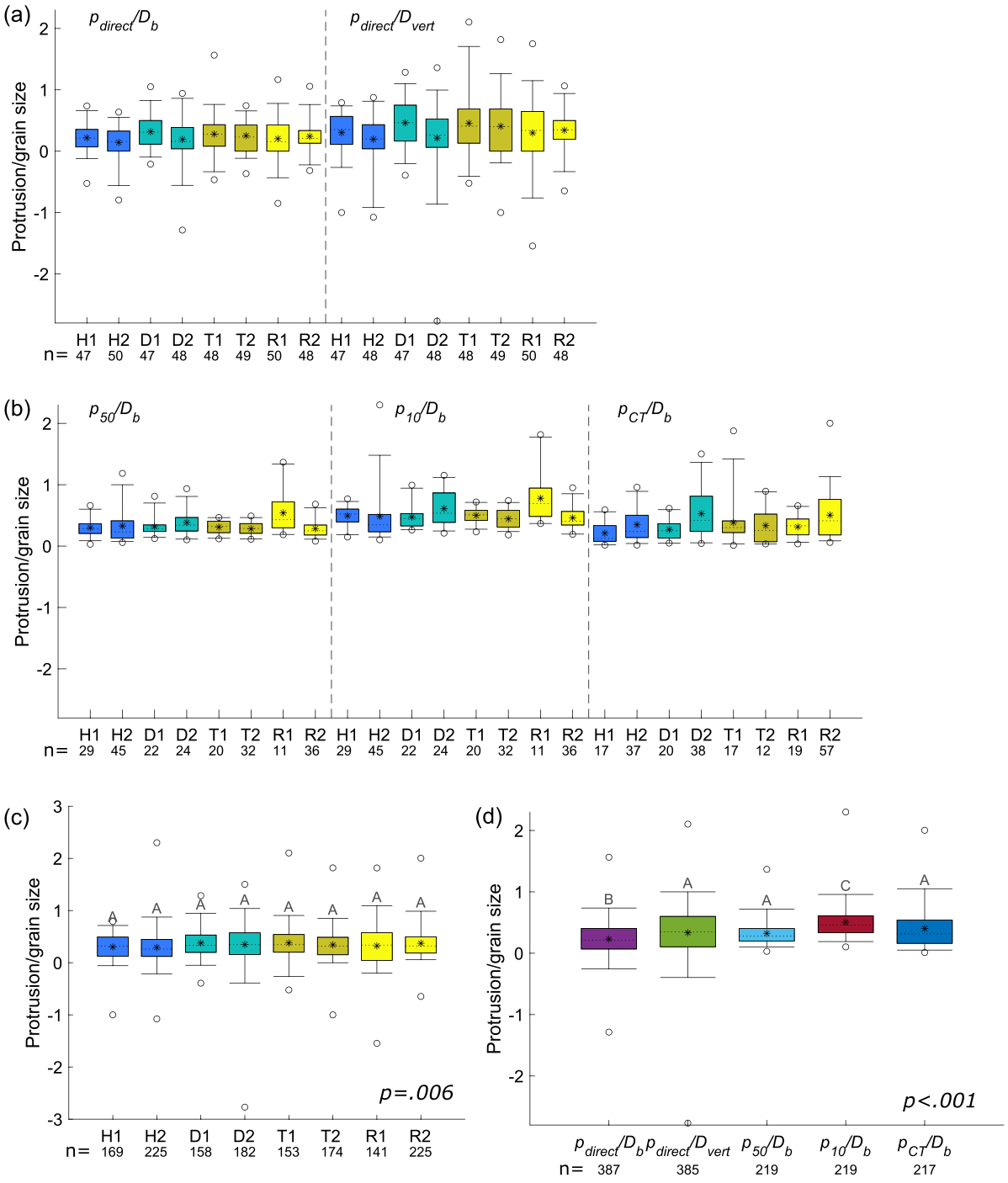

FIGURE 4 Protrusion measurements. (a) and (b) Protrusion relative to grain size, calculated from direct measurements (p_{direct}/D_b and p_{direct}/D_{vert}), Terrestrial Laser Scanning data (p_{50}/D_b and p_{10}/D_b) and Computed Tomography data (p_{CT}/D_b). (c) The same data grouped by patch; (d) the same data grouped by method. In all panels H: pool head; D: pool deep; T: pool tail; and R: riffle. 1 are the upstream patches, and 2 are the downstream patches. Boxplots show 25th to 75th percentiles, dashed line is the median, whiskers show 5th and 95th percentiles, open circles show min and max, and star is the mean. *n* indicates number of grains in each distribution. In the combined data from (a) and (b), the Scheirer–Ray–Hare test shows significant differences between patches and between methods. In (c) and (d), groups sharing a capital letter are not significantly different as identified by post-hoc Dunn test, although no significant differences were identified between patches despite the significant Scheirer–Ray–Hare result. [Color figure can be viewed at wileyonlinelibrary.com]

4.2.2 | Grain size, orientation and surface roughness

Grain size was collected using three different approaches: direct measurements, TLS data and CT data. D_{50} (median of D_b) from direct measurements ranges from 30 to 45 mm, D_{50} from G3Point analysis of TLS data is similar at 28 to 48 mm (reflecting the role of the field data in constraining G3Point parameters), but D_{50} from CT data is smaller at 9 to 41 mm (Figure 3a). The Scheirer–Ray–Hare test shows that both method and patch location produce significant differences in grain size ($p < 0.001$ for both), but the interaction term is insignificant ($p = 0.436$). CT results are significantly finer than the other two

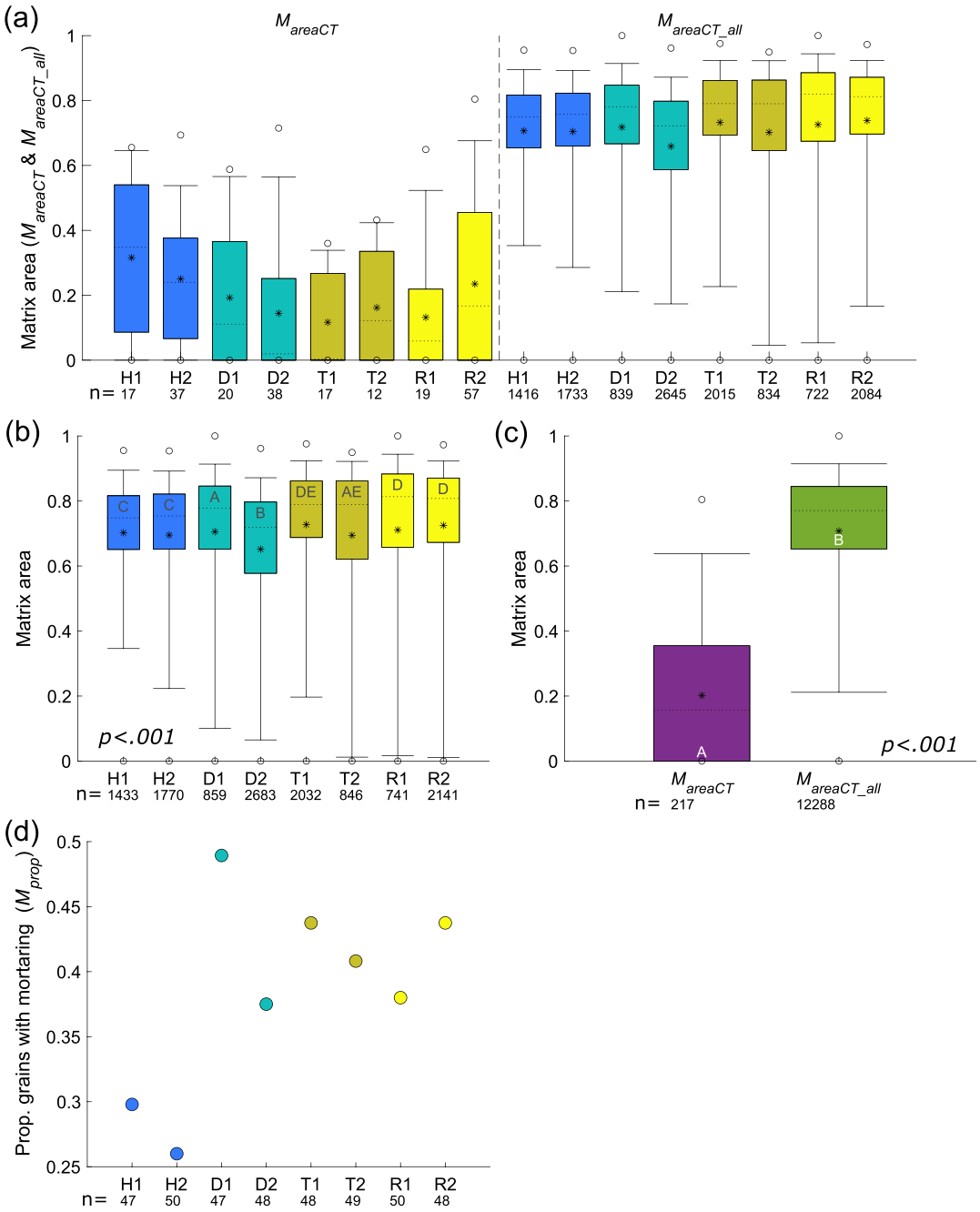

FIGURE 5 Matrix measurements. (a) and (b) Matrix calculated from Computed Tomography data for surface grains (M_{areaCT}) and all grains (M_{areaCT_all}). (c) The same data grouped by patch; (d) the same data grouped by method. In all panels, H: pool head; D: pool deep; T: pool tail; and R: riffle. 1 are the upstream patches, and 2 are the downstream patches. Boxplots show 25th to 75th percentiles, dashed line is the median, whiskers show 5th and 95th percentiles, open circles show min and max, and star is the mean. *n* indicates number of grains in each distribution. For the data in (a), the Scheirer–Ray–Hare test shows significant differences between patches and between methods. In (b) and (c), groups sharing a capital letter are not significantly different as identified by post-hoc Dunn test. [Color figure can be viewed at wileyonlinelibrary.com]

methods (Dunn test, Figure 3c). Across all methods, the downstream patch of each unit is significantly finer than the upstream one (Dunn test, Figure 3b), but there is no significant difference in size across all upstream units (Dunn test, Figure 3b). Bed roughness, σ_z, generally decreases from pool deep (D), to pool tail (T), to riffles (R), with large variation in pool heads (second highest and lowest values; Figure 3d). For each unit, σ_z is lower for the downstream patch, which is consistent with those patches having smaller grain sizes as shown by the previous data. In all patches, most grains are arranged with their *c*-axis vertical with no significant differences between patches (Chi-square test, $p = 0.32$, Figure 3e).

4.2.3 | Protrusion

The Scheirer–Ray–Hare test shows that protrusion varies significantly with patch ($p = 0.006$), method ($p < 0.001$) and the interaction between them ($p = 0.040$). Using the Dunn test to compare only by method, the distributions of values of p_{direct}/D_{vert}, p_{50}/D_b and p_{CT}/D_b are not significantly different (Figure 4a, b and d). The medians of p_{direct}/D_{vert} are 0.20 to 0.46, those of p_{50}/D_b are 0.23 to 0.43, and those of p_{CT}/D_b are 0.12 to 0.42. This similarity is despite D_{vert} being the *c*-axis for most grains, rather than the *b*-axis that is used in the TLS and CT measurements. For the two methods with significant

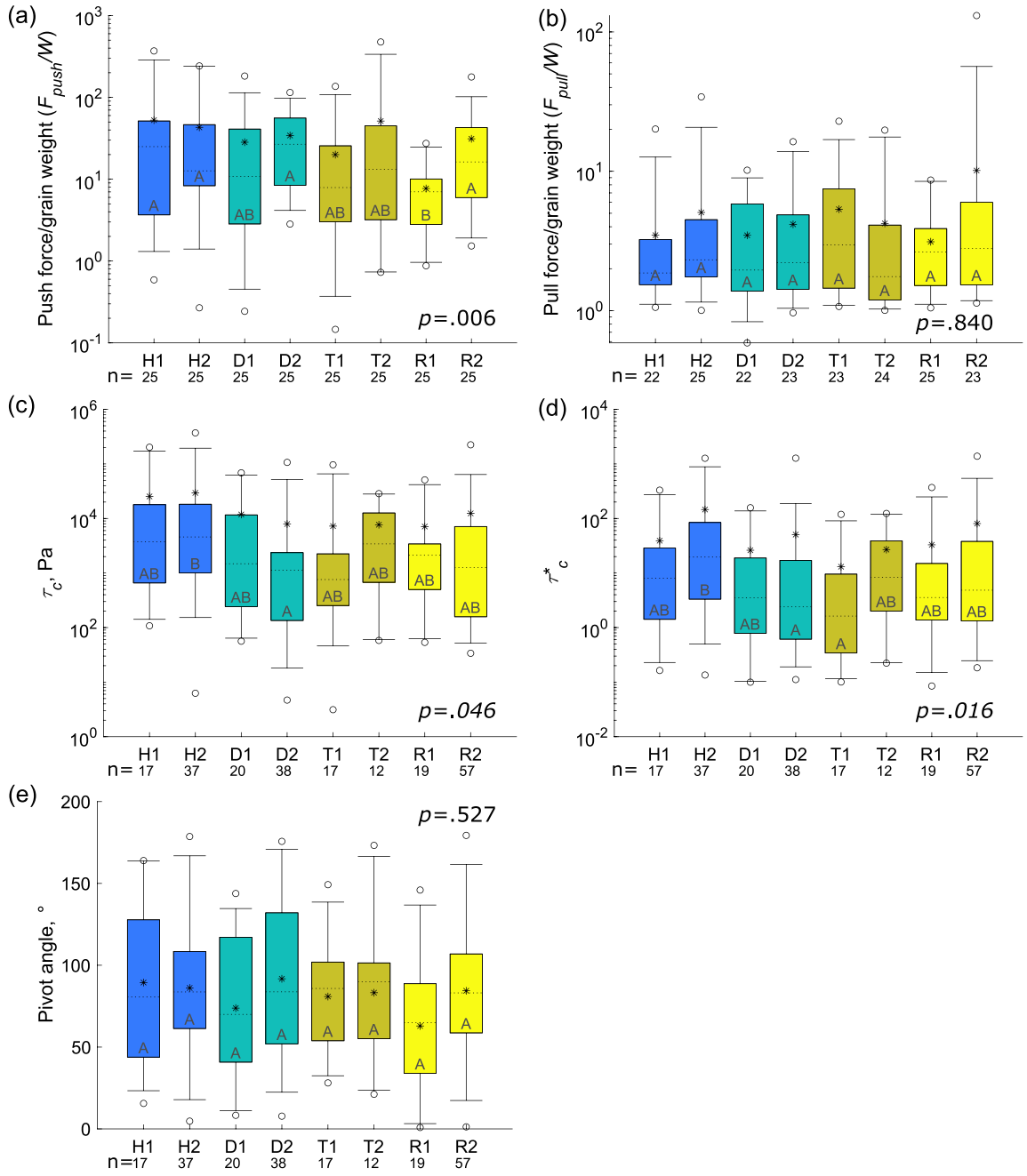

FIGURE 6 Forces and shear stresses. (a) Push forces normalised by grain weight (F_{push}/W) and (b) pull forces normalised by grain weight (F_{pull}/W) measured in the field; (c) modelled critical shear stress (τ_c), (d) modelled dimensionless critical shear stress (τ^*_c), and (e) pivot angle measured from Computed Tomography data. In all panels H: pool head; D: pool deep; T: pool tail; and R: riffle. 1 are the upstream patches, and 2 are the downstream patches. Boxplots show 25th to 75th percentiles, dashed line is the median, whiskers show 5th and 95th percentiles, open circles show min and max, and star is the mean. *n* indicates number of grains in each distribution. The *p*-values are from a Kruskal–Wallis test for difference between the distributions. Where there are significant differences ($p < 0.05$), groups sharing a capital letter are not significantly different as identified by post-hoc Dunn test. [Color figure can be viewed at wileyonlinelibrary.com]

differences, values of p_{direct}/D_b are comparatively lower (0.16 to 0.31), and values of p_{10}/D_b are higher (0.34 to 0.70) because of the lower bed elevation that protrusion is calculated relative to. Compared to the other methods, the direct measurements have a larger proportion of negative protrusion values, which indicate that the grain does not protrude above the surrounding grains. Despite the Scheirer–Ray–Hare test showing a significant difference between patches, using the Dunn test to compare only by patch shows no significant differences (Figure 4c).

4.2.4 | Fine-grained matrix

Using the Scheirer–Ray–Hare test, the proportion of grain surface that is in contact with fine-grained matrix varies significantly with both patch ($p < 0.001$) and method ($p < 0.001$) but not the interaction between them ($p = 0.135$). The differences between the methods depends on whether just surface grains are measured (M_{areaCT}, median value of < 0.4) or all grains (M_{areaCT_all}, median value of ~0.8) (Figure 5a and c). Using the Dunn test to compare by patch shows

that the upstream and downstream patches of each unit are not significantly different (apart from pool deep units), with lowest values in the pool heads and highest values in the riffles and pool tail (Figure 5b). These distributions are, however, dominated by M_{areaCT_all} because of the difference in sample size. For M_{areaCT}, the pool heads actually have the highest values. The proportion of grains where matrix was noted in the direct measurements (M_{prop}) varies from 0.26 to about 0.49 (Figure 5d). Like M_{areaCT_all}, M_{prop} is lowest for the pool head patches (H1 and H2), and other units have higher values.

4.2.5 | Dislodgement forces and critical shear stress

There are few consistent patterns in the data for dislodgement forces and τ_c. Push force normalised by grain weight (F_{push}/W) is significantly different between patches (Kruskal–Wallis, $p = 0.006$, Figure 6a), whereas pull force normalised by grain weight (F_{pull}/W) is not (Kruskal–Wallis, $p = 0.840$, Figure 6b). However, for F_{push}/W, the Dunn test shows that seven patches are not significantly different to each other, and the remaining patch R1 is not significantly different to three patches. Values of τ_c and τ^*_c calculated using a moment balance model are also significantly different between patches (Kruskal–Wallis, $p = 0.046$ and 0.016, respectively; Figure 6c and d), but the Dunn test shows that for τ_c only two patches (H2 and D2) are significantly different from each other. τ^*_c shows a similar result, with only three patches (H2, D2 and T1) being significantly different to some other patches. For each unit, there is no consistent pattern as to whether τ_c and τ^*_c are highest upstream or downstream. Pivot angles calculated from CT scans do not vary systematically between the patches (Kruskal–Wallis, $p = 0.527$; Figure 6e).

4.3 | Comparison between all three approaches

For each of the different variables, there is an agreement between some methods and not between other methods. For example, there is similarity between direct and TLS measurements of D_b, similarity between direct (p_{direct}/D_{vert}), TLS (p_{50}/D_b) and CT (p_{CT}/D_b) measurements of protrusion, and similarity between direct (M_{prop}) and CT (M_{areaCT_all}) measurements of fine-grained matrix. To extend this analysis, we now compare between different variables to establish which variables have a significant correlation (Figure 7). In this analysis, for variables where we recorded a distribution, we use the median value.

Relatively few variables are significantly related to each other, though this may reflect the small number of patches and the fairly small sample sizes of some variables (e.g. direct field measurements). In agreement with earlier analysis, there is broad agreement between different ways of measuring grain size, with significant correlations between most combinations of direct D_b, TLS D_b, CT D_b and TLS σ_z. Comparing protrusion to grain size for each method, the direct field data show no correlation between the two, TLS data show significant positive correlation, whereas CT data exhibit significant negative correlation. Consequently, and contrary to our earlier analysis, no correlation exists between any protrusion data for direct, TLS and CT datasets (which may show the limitation of comparing medians and not distributions). TLS σ_z does not correlate significantly for any measure of protrusion, suggesting its variation is predominantly controlled by grain size.

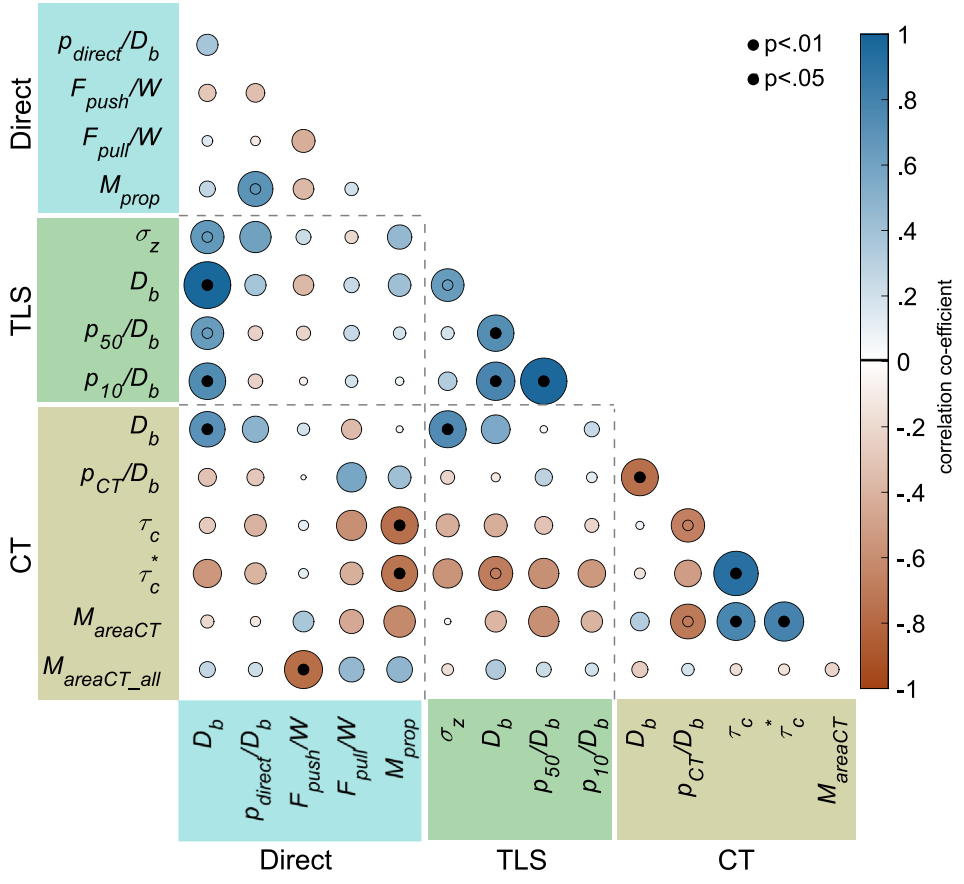

FIGURE 7 Cross-correlation analysis of 14 variables collected using direct measurements, Terrestrial Laser Scanning and Computed Tomography data. Circle size and colour show the correlation coefficient. Overlying black open circles indicate a significant correlation at $p < 0.05$, and filled black circles indicate $p < 0.01$. [Color figure can be viewed at wileyonlinelibrary.com]

Little agreement exists between different ways of measuring the fine-grain matrix, with no significant correlations among M_{prop}, M_{areaCT} and M_{areaCT_all} (again contrary to previous analysis). τ_c and τ^*_c have an expected positive correlation with each other, and a significant positive correlation with M_{areaCT}. The latter is because the cohesive resistant force produced by the matrix is incorporated in modelled values of τ_c. Both τ_c and τ^*_c have a significant negative correlation with M_{prop}, which is consistent with the negative correlation between direct and M_{areaCT} measurements.

4.4 | Summary

The similarity between the three methods varies between different parameters. All methods identified consistent patterns in grain size between upstream and downstream patches (Figure 3a), which were also identified by TLS σ_z (Figure 3e). This is despite each method using a different grain sampling strategy, with smaller grains being more likely to be sampled in the CT data (Figure 3c). Although measurements were taken from the same area of the bed, we were unable to compare measurements from the exact same grains.

There is less consistency between the different methods for both protrusion and matrix amount. Three out of five protrusion methods produce similar distributions of protrusion values. However, there was no systematic variation in protrusion values between patches for the different methods, reflecting both different definitions of protrusion and individual method limitations. For direct protrusion measurements, it can be difficult to define the bed elevation that protrusion should be measured relative to and hence where to best place a ruler adjacent to the measured grain. Such measurements are also time consuming, hence our fairly small sample sizes. For TLS data and G3Point/Pro+, grain identification is uncertain, and protrusion values are sensitive to the method of parameterisation (Yager et al., 2024). For CT data, the method requires an upstream area around each grain of a length equivalent to D_{84} for protrusion to be measured relative to. The relatively small basket diameters meant that protrusion calculations for grains close to the upstream edge were unattainable, so we artificially extended the surface using duplicate images of the basket topography around the basket. The displacement of grains at the basket edge during excavation may also affect the measured protrusions. From this comparison, it is difficult to know which is the most accurate method. In terms of ease of application, point cloud-based methods were the most potential.

Measurements of matrix also differ between CT and field data. As with protrusion, the differences likely reflect different definitions and methodological limitations. Both M_{prop} and M_{areaCT} were measured for only surface grains, but M_{prop} identified higher levels of matrix contact than M_{areaCT}. This suggests that matrix may have been accidentally removed from the surface grains during the basket excavation and/or wax stabilisation process. Alternatively, the similarity between M_{prop} and M_{areaCT_all} may suggest that the M_{prop} observations better reflect the subsurface rather than the surface conditions. Furthermore, M_{prop} just recorded the presence/absence for each grain and does not quantify the amount of matrix. Accurate estimates of the amount of fine-grained matrix in the bed are important given the impact of this parameter on modelled values of τ_c, but, as with protrusion, it is difficult to know which is the most accurate method.

5 | CONCLUSIONS

5.1 | Measuring τ_c

New methods for measuring both bulk bedload transport and the movement of individual grains provide new opportunities for quantifying spatial and temporal variations in τ_c across a wider range of rivers. However, at present, most of these methods are best at calculating reach-averaged values of τ_c unless they are coupled with measured or modelled values of local shear stresses. New datasets have built on earlier observations that τ_c is not a fixed value and rather should be treated as a state function that varies in space and time (Hassan, Saletti, Johnson, et al., 2020; Johnson, 2016). There is a need for more measurements of bedload from a wider range of rivers, using techniques such as seismic or impact plate monitoring. Such data would enable us to measure how the magnitude and frequency of changes in τ_c differ between channels and to start identifying the role of different drivers in these changes. The selection of rivers for such a survey should also take into account factors such as channel morphology and slope, which have not been considered here. To identify spatial changes in τ_c within a river channel, advances in grain location tracking are needed so that we can record the location of instrumented grains as well as when they move. Another useful advance would also be the ability to collect data wirelessly from the grains while they are in the channel. Many instrumented grains currently need to be retrieved to download the data, risking data loss if grains cannot be found.

5.2 | Measuring sediment structure

The three different methods we presented show that there is growing potential to measure sediment structure in the field. However, there is inconsistency between the different approaches, and no single approach yet offers an easy solution to quantifying structural metrics. Methods for calculating surface grain size and protrusion distributions from bed topography, such as G3Point/Pro+ (Steer et al., 2022; Yager et al., 2024), have substantial potential given that TLS and SfM photogrammetry data can be collected quickly and from large areas of a channel, but further development and testing is needed. Such methods should also be applicable to data collected from submerged areas of the bed, as the current focus on exposed areas may limit the representativeness of the resulting data. Current approaches are also limited by the inability to quantify how structure changes within an event, as only pre- or post-event metrics can be determined. We have also shown that fine-grained matrix can affect τ_c values. It is less likely that the amount of matrix could be estimated from topographic data, and direct field observations may be required. Another approach could be to employ models that predict the amount of fine sediment in the bed as a function of flow characteristics (Czuba et al., 2022). It also remains unclear if the control of grain interlocking (intergranular friction) on τ_c can be accurately inferred from surface topography (e.g. Yager, Schmeeckle, & Badoux, 2018).

One factor that is also expected to affect τ_c, but which we have not yet considered in this review, is the effect of biological organisms. Some organisms such as caddis fly and mussels increase τ_c by providing additional cohesion which inhibits grain motion (Albertson

et al., 2014; Johnson et al., 2009; Sanders et al., 2022), whereas others such as crayfish and fish disrupt the bed, decreasing τ_c (Buxton et al., 2015; Johnson et al., 2011; Pledger et al., 2014). As both involve changes to sediment structure, new methods to link structure to τ_c could also help to quantify the impacts of different organisms. For example, Buxton et al. (2015) demonstrated that simulated spawning in a laboratory flume caused a measured decrease in τ_c compared to unspawned locations. This change in τ_c was related to lower measured push entrainment forces on the spawned versus the unspawned beds.

5.3 | Next steps

There are clear advances to be made in both measuring bedload transport and quantifying sediment structure. Addressing each of these areas individually will contribute to our understanding of, and ability to predict, sediment entrainment. However, further advances could be made by combining these two areas, for example, a study in a channel with regular high flow events that identifies when sediment moves and how channel bed conditions vary over time. Such a study could include direct measurements of grain dislodgement forces and repeated high-resolution surveys of the channel bed during intervening low flow periods, and thus compare changes in bed topography with changing dislodgment forces. Such data could then be compared to temporal differences in τ_c identified from analysis of bedload transport data. There is also a need for further testing of methods to measure sediment structure to determine which are most appropriate and accurate. More generally, while it may not always be practical or possible to measure sediment structure in order to predict τ_c, improved understanding of how sediment structure changes and consequently controls bedload entrainment will enable the development of new predictive relationships for τ_c and a more mechanistic understanding of associated uncertainties.

ACKNOWLEDGEMENTS

RAH, HEV, JL and DAS acknowledge funding from the Natural Environment Research Council, grant numbers NE/K012304/1 and NE/K013386/1. EY acknowledges funding from the US National Science Foundation, grant EAR1921790. Thanks to the organisers of Gravel Bed Rivers 9 for the invitation to present this work, and thanks to all attendees for the informative discussions. Thanks to the reviewers and the AE for their feedback on the paper.

DATA AVAILABILITY STATEMENT

The TLS and CT data from Bury Green Brook are available from Hodge et al. (2022): https://doi.org/10.5285/b30b4d56-f0a9-43e8-aacc-09d9b5b1f9fc. Data from Figures 3 to 6 are available on Zenodo: https://zenodo.org/doi/10.5281/zenodo.10403314.

ORCID

Rebecca A. Hodge https://orcid.org/0000-0002-8792-8949
Hal E. Voepel https://orcid.org/0000-0001-7375-1460
Elowyn M. Yager https://orcid.org/0000-0002-3382-2356

REFERENCES

Aberle, J. & Smart, G.M. (2003) The influence of roughness structure on flow resistance on steep slopes. *Journal of Hydraulic Research*, 41(3), 259–269. Available from: https://doi.org/10.1080/00221680309499971

Adams, D.L. & Eaton, B.C. (2022) A comparison of 1D and 2D bedload transport functions under high excess shear stress conditions in laterally constrained gravel-bed rivers: a laboratory study. *Earth Surface Dynamics*, 10(5), 895–907. Available from: https://doi.org/10.5194/esurf-10-895-2022

Aigner, J., Kreisler, A., Rindler, R., Hauer, C. & Habersack, H. (2017) Bedload pulses in a hydropower affected alpine gravel bed river. *Geomorphology*, 291, 116–127. Available from: https://doi.org/10.1016/j.geomorph.2016.05.015

Albertson, L.K., Sklar, L.S., Pontau, P., Dow, M. & Cardinale, B.J. (2014) A mechanistic model linking insect (Hydropsychidae) silk nets to incipient sediment motion in gravel-bedded streams. *Journal of Geophysical Research: Earth Surface*, 119(9), 1833–1852. Available from: https://doi.org/10.1002/2013JF003024

Amon, A., Born, P., Daniels, K.E., Dijksman, J.A., Huang, K., Parker, D., et al. (2017) Preface: focus on imaging methods in granular physics. *Review of Scientific Instruments*, 88(5), 051701. Available from: https://doi.org/10.1063/1.4983052

Ancey, C. (2020) Bedload transport: a walk between randomness and determinism. Part 1. The state of the art. *Journal of Hydraulic Research*, 58(1), 1–17. Available from: https://doi.org/10.1080/00221686.2019.1702594

Anthony, R.E., Aster, R.C., Ryan, S., Rathburn, S. & Baker, M.G. (2018) Measuring mountain river discharge using seismographs emplaced within the hyporheic zone. *Journal of Geophysical Research: Earth Surface*, 123(2), 210–228. Available from: https://doi.org/10.1002/2017JF004295

National River Flow Archive. (2023) *38002 - Ash at Mardock [online]*. Available from: https://nrfa.ceh.ac.uk/data/station/info/38002 [Accessed 23th February 2023].

Bakker, M., Gimbert, F., Geay, T., Misset, C., Zanker, S. & Recking, A. (2020) Field application and validation of a seismic bedload transport model. *Journal of Geophysical Research: Earth Surface*, 125(5), e2019JF005416. Available from: https://doi.org/10.1029/2019JF005416

Barrière, J., Oth, A., Hostache, R. & Krein, A. (2015) Bedload transport monitoring using seismic observations in a low-gradient rural gravel-bed stream. *Geophysical Research Letters*, 42(7), 2294–2301. Available from: https://doi.org/10.1002/2015GL063630

Barzilai, R., Laronne, J.B. & Reid, I. (2012) Effect of changes in fine-grained matrix on bedload sediment transport in a gravel-bed river. *Earth Surface Processes and Landforms*, 38(5), 441–448. Available from: https://doi.org/10.1002/esp.3288

Bertin, S. & Friedrich, H. (2016) Field application of close-range digital photogrammetry (CRDP) for grain-scale fluvial morphology studies. *Earth Surface Processes and Landforms*, 41(10), 1358–1369. Available from: https://doi.org/10.1002/esp.3906

Beylich, A.A. & Laute, K. (2014) Combining impact sensor field and laboratory flume measurements with other techniques for studying fluvial bedload transport in steep mountain streams. *Geomorphology*, 218, 72–87. Available from: https://doi.org/10.1016/j.geomorph.2013.09.004

Biggs, H., Starr, A., Smith, B., de Lima, S., Sykes, J., Haddadchi, A., et al. (2022) Kinematic loggers—development of rugged sensors and recovery systems for field measurements of stone rolling dynamics and impact accelerations during floods. *Sensors*, 22(3), 1013. Available from: https://doi.org/10.3390/s22031013

Booth, A.M., Hurley, R., Lamb, M.P. & Andrade, J.E. (2014) Force chains as the link between particle and bulk friction angles in granular material. *Geophysical Research Letters*, 41(24), 8862–8869. Available from: https://doi.org/10.1002/2014GL061981

Bradley, D.N. & Tucker, G.E. (2013) The storage time, age, and erosion hazard of laterally accreted sediment on the floodplain of a simulated meandering river. *Journal of Geophysical Research: Earth Surface*, 118(3), 1308–1319. Available from: https://doi.org/10.1002/jgrf.20083

Buffington, J.M., Dietrich, W.E. & Kirchner, J.W. (1992) Friction angle measurements on a naturally formed gravel streambed—implications for

critical boundary shear-stress. *Water Resources Research*, 28(2), 411–425. Available from: https://doi.org/10.1029/91WR02529

Buffington, J.M. & Montgomery, D.R. (1997) A systematic analysis of eight decades of incipient motion studies, with special reference to gravel-bedded rivers. *Water Resources Research*, 33(8), 1993–2029. Available from: https://doi.org/10.1029/96WR03190

Burtin, A., Bollinger, L., Vergne, J., Cattin, R. & Nábělek, J.L. (2008) Spectral analysis of seismic noise induced by rivers: a new tool to monitor spatiotemporal changes in stream hydrodynamics. *Journal of Geophysical Research: Solid Earth*, 113(B5), B05301. Available from: https://doi.org/10.1029/2007JB005034

Butler, J.B., Lane, S.N. & Chandler, J.H. (1998) Assessment of DEM quality for characterizing surface roughness using close range digital photogrammetry. *The Photogrammetric Record*, 16(92), 271–291. Available from: https://doi.org/10.1111/0031-868X.00126

Butler, J.B., Lane, S.N. & Chandler, J.H. (2001) Characterization of the structure of river-bed gravels using two-dimensional fractal analysis. *Mathematical Geology*, 33, 301–330. Available from: https://doi.org/10.1023/A:1007686206695

Buxton, T.H., Buffington, J.M., Yager, E.M., Hassan, M.A. & Fremier, A.K. (2015) The relative stability of salmon redds and unspawned streambeds. *Water Resources Research*, 51(8), 6074–6092. Available from: https://doi.org/10.1002/2015WR016908

Carrivick, J.L. & Smith, M.W. (2019) Fluvial and aquatic applications of structure from motion photogrammetry and unmanned aerial vehicle/drone technology. *WIREs Water*, 6(1), e1328. Available from: https://doi.org/10.1002/wat2.1328

Cassel, M., Navratil, O., Perret, F. & Piégay, H. (2021) The e-RFIDuino: an Arduino-based RFID environmental station to monitor mobile tags. *HardwareX*, 10, e00210. Available from: https://doi.org/10.1016/j.ohx.2021.e00210

Cassel, M., Piégay, H., Fantino, G., Lejot, J., Bultingaire, L., Michel, K., et al. (2020) Comparison of ground-based and UAV a-UHF artificial tracer mobility monitoring methods on a braided river. *Earth Surface Processes and Landforms*, 45(5), 1123–1140. Available from: https://doi.org/10.1002/esp.4777

Casserly, C.M., Turner, J.N., O' Sullivan, J.J., Bruen, M., Magee, D., Coiléir, S.O., et al. (2021) Coarse sediment dynamics and low-head dams: monitoring instantaneous bedload transport using a stationary RFID antenna. *Journal of Environmental Management*, 300, 113671. Available from: https://doi.org/10.1016/j.jenvman.2021.113671

Celik, A.O., Diplas, P. & Dancey, C.L. (2013) Instantaneous turbulent forces and impulse on a rough bed: implications for initiation of bed material movement. *Water Resources Research*, 49(4), 2213–2227. Available from: https://doi.org/10.1002/wrcr.20210

Chao, W.-A., Wu, Y.-M., Zhao, L., Tsai, V.C. & Chen, C.-H. (2015) Seismologically determined bedload flux during the typhoon season. *Scientific Reports*, 5(1), 8261. Available from: https://doi.org/10.1038/srep08261

Charru, F., Mouilleron, H. & Eiff, O. (2004) Erosion and deposition of particles on a bed sheared by a viscous flow. *Journal of Fluid Mechanics*, 519, 55–80. Available from: https://doi.org/10.1017/S0022112004001028

Cook, K.L., Andermann, C., Gimbert, F., Adhikari, B.R. & Hovius, N. (2018) Glacial lake outburst floods as drivers of fluvial erosion in the Himalaya. *Science*, 362(6410), 53–57. Available from: https://doi.org/10.1126/science.aat4981

Cook, K.L. & Dietze, M. (2022) Seismic advances in process geomorphology. *Annual Review of Earth and Planetary Sciences*, 50(1), 183–204. Available from: https://doi.org/10.1146/annurev-earth-032320-085133

Coussot, P. (2020) Progress in rheology and hydrodynamics allowed by NMR or MRI techniques. *Experiments in Fluids*, 61(9), 207. Available from: https://doi.org/10.1007/s00348-020-03037-y

Cúñez, F.D., Franklin, E.M., Houssais, M., Arratia, P. & Jerolmack, D.J. (2022) Strain hardening by sediment transport. *Physical Review Research*, 4(2), L022055. Available from: https://doi.org/10.1103/PhysRevResearch.4.L022055

Curran, J.C. & Tan, L. (2014) Effect of bed sand content on the turbulent flows associated with clusters on an armored gravel bed surface. *Journal of Hydraulic Engineering*, 140(2), 137–148. Available from: https://doi.org/10.1061/(ASCE)HY.1943-7900.0000810

Curran, J.C. & Waters, K.A. (2014) The importance of bed sediment sand content for the structure of a static armor layer in a gravel bed river. *Journal of Geophysical Research: Earth Surface*, 119(7), 1484–1497. Available from: https://doi.org/10.1002/2014JF003143

Czuba, J.A., Hirschler, M., Pratt, E.A., Villamagna, A. & Angermeier, P.L. (2022) Bankfull shear velocity predicts embeddedness and silt cover in gravel streambeds. *River Research and Applications*, 38(1), 59–68. Available from: https://doi.org/10.1002/rra.3878

Deal, E., Venditti, J.G., Benavides, S.J., Bradley, R., Zhang, Q., Kamrin, K., et al. (2023) Grain shape effects in bed load sediment transport. *Nature*, 613(7943), 298–302. Available from: https://doi.org/10.1038/s41586-022-05564-6

Detert, M. & Weitbrecht, W. (2012) Automatic object detection to analyze the geometry of gravel grains – a free stand-alone tool. In: Muños, R.M. (Ed.) *River Flow*. London: Taylor & Francis, pp. 595–600.

Dietrich, W.E., Kirchner, J.W., Ikeda, H. & Iseya, F. (1989) Sediment supply and the development of the coarse surface layer in gravel-bedded rivers. *Nature*, 340(6230), 215–217. Available from: https://doi.org/10.1038/340215a0

Dini, B., Bennett, G.L., Franco, A.M.A., Whitworth, M.R.Z., Cook, K.L., Senn, A., et al. (2021) Development of smart boulders to monitor mass movements via the internet of things: a pilot study in Nepal. *Earth Surface Dynamics*, 9(2), 295–315. Available from: https://doi.org/10.5194/esurf-9-295-2021

Diplas, P., Dancey, C.L., Celik, A.O., Valyrakis, M., Greer, K. & Akar, T. (2008) The role of impulse on the initiation of particle movement under turbulent flow conditions. *Science*, 322(5902), 717–720. Available from: https://doi.org/10.1126/science.1158954

Dobson, D.W., Todd Holland, K. & Calantoni, J. (2014) Fast, large-scale, particle image velocimetry-based estimations of river surface velocity. *Computers & Geosciences*, 70, 35–43. Available from: https://doi.org/10.1016/j.cageo.2014.05.007

Downs, P.W. & Soar, P.J. (2021) Beyond stationarity: influence of flow history and sediment supply on coarse bedload transport. *Water Resources Research*, 57(2), e2020WR027774. Available from: https://doi.org/10.1029/2020WR027774

Dunn, O.J. (1964) Multiple comparisons using rank sums. *Technometrics*, 6(3), 241–252. Available from: https://doi.org/10.1080/00401706.1964.10490181

Eltner, A., Bertalan, L., Grundmann, J., Perks, M.T. & Lotsari, E. (2021) Hydro-morphological mapping of river reaches using videos captured with UAS. *Earth Surface Processes and Landforms*, 46(14), 2773–2787. Available from: https://doi.org/10.1002/esp.5205

Emmett, W.W. (1980) *A field calibration of the sediment-trapping characteristics of the Helley-Smith bed-load sampler*. USGS: USGS Numbered Series.

Ergenzinger, P., Schmidt, K.-H. & Busskamp, R. (1989) The pebble transmitter system (PETS): first results of a technique for studying coarse material erosion, transport and deposition. *Zeitschrift für Geomorphologie*, 33(4), 503–508. Available from: https://doi.org/10.1127/zfg/33/1989/503

Feehan, S.A., McCoy, S.W., Scheingross, J.S. & Gardner, M.H. (2023) Quantifying variability of incipient-motion thresholds in gravel-bedded rivers using a grain-scale force-balance model. *Journal of Geophysical Research: Earth Surface*, 128(9), e2023JF007162. Available from: https://doi.org/10.1029/2023JF007162

Fenton, J.D. & Abbott, J.E. (1977) Initial movement of grains on a stream bed - effect of relative protrusion. *Proceedings of the Royal Society of London Series A-Mathematical*, 352(1671), 523–537. Available from: https://doi.org/10.1098/rspa.1977.0014

Ferguson, R.I. (2003) The missing dimension: effects of lateral variation on 1-D calculations of fluvial bedload transport. *Geomorphology*, 56(1-2), 1–14. Available from: https://doi.org/10.1016/S0169-555X(03)00042-4

Ferguson, R.I., Bloomer, D.J., Hoey, T.B. & Werritty, A. (2002) Mobility of river tracer pebbles over different timescales. *Water Resources Research*, 38(5), Available from: https://doi.org/10.1029/2001WR000254

Ferguson, R.I. & Hoey, T.B. (2002) Long-term slowdown of river tracer pebbles: generic models and implications for interpreting short-term tracer studies. *Water Resources Research*, 38(8), Available from: https://doi.org/10.1029/2001WR000637

Ferguson, R., Hoey, T., Wathen, S. & Werritty, A. (1996) Field evidence for rapid downstream fining of river gravels through selective transport. *Geology*, 24(2), 179–182. Available from: https://doi.org/10.1130/0091-7613(1996)024<0179:FEFRDF>2.3.CO;2

Ferguson, R.I., Sharma, B.P., Hodge, R.A., Hardy, R.J. & Warburton, J. (2017) Bed load tracer mobility in a mixed bedrock/alluvial channel: tracer-pebble mobility over bedrock. *Journal of Geophysical Research: Earth Surface*, 122(4), 807–822. Available from: https://doi.org/10.1002/2016JF003946

Fujita, I., Muste, M. & Kruger, A. (1998) Large-scale particle image velocimetry for flow analysis in hydraulic engineering applications. *Journal of Hydraulic Research*, 36(3), 397–414. Available from: https://doi.org/10.1080/00221689809498626

Galanis, M., Shattuck, M.D., O'Hern, C.S. & Ouellette, N.T. (2022) Directional strengthening and weakening in hydrodynamically sheared granular beds. *Physical Review Fluids*, 7(1), 013802. Available from: https://doi.org/10.1103/PhysRevFluids.7.013802

Geay, T., Zanker, S., Misset, C. & Recking, A. (2020) Passive acoustic measurement of bedload transport: toward a global calibration curve? *Journal of Geophysical Research: Earth Surface*, 125(8), e2019JF005242. Available from: https://doi.org/10.1029/2019JF005242

Gimbert, F., Fuller, B.M., Lamb, M.P., Tsai, V.C. & Johnson, J.P.L. (2018) Particle transport mechanics and induced seismic noise in steep flume experiments with accelerometer-embedded tracers: experimental testing of seismic noise generated by sediment transport. *Earth Surface Processes and Landforms*, 44(1), 219–241. Available from: https://doi.org/10.1002/esp.4495

Gimbert, F., Tsai, V.C. & Lamb, M.P. (2014) A physical model for seismic noise generation by turbulent flow in rivers. *Journal of Geophysical Research: Earth Surface*, 119(10), 2209–2238. Available from: https://doi.org/10.1002/2014JF003201

Goode, J.R. & Wohl, E. (2010) Coarse sediment transport in a bedrock channel with complex bed topography. *Water Resources Research*, 46(11), W11532. Available from: https://doi.org/10.1029/2009WR008135

Govi, M., Maraga, F. & Moia, F. (1993) Seismic detectors for continuous bed load monitoring in a gravel stream. *Hydrological Sciences Journal*, 38(2), 123–132. Available from: https://doi.org/10.1080/02626669309492650

Graham, D.J., Reid, I. & Rice, S.P. (2005) Automated sizing of coarse-grained sediments: image-processing procedures. *Mathematical Geology*, 37(1), 1–28. Available from: https://doi.org/10.1007/s11004-005-8745-x

Habersack, H.M. (2001) Radio-tracking gravel particles in a large braided river in New Zealand: a field test of the stochastic theory of bed load transport proposed by Einstein. *Hydrological Processes*, 15(3), 377–391. Available from: https://doi.org/10.1002/hyp.147

Habersack, H., Hein, T., Stanica, A., Liska, I., Mair, R., Jäger, E., et al. (2016) Challenges of river basin management: current status of, and prospects for, the river Danube from a river engineering perspective. *Science of the Total Environment*, 543(Pt A), 828–845. Available from: https://doi.org/10.1016/j.scitotenv.2015.10.123

Habersack, H., Kreisler, A., Rindler, R., Aigner, J., Seitz, H., Liedermann, M., et al. (2017) Integrated automatic and continuous bedload monitoring in gravel bed rivers. *Geomorphology*, 291, 80–93. Available from: https://doi.org/10.1016/j.geomorph.2016.10.020

Hart, J.K. & Martinez, K. (2022) Sensor Networks and Geohazards. In: *Treatise on Geomorphology*. London: Elsevier, pp. 100–120.

Haschenburger, J.K. (2013) Tracing river gravels: insights into dispersion from a long-term field experiment. *Geomorphology*, 200, 121–131. Available from: https://doi.org/10.1016/j.geomorph.2013.03.033

Hassan, M.A. & Reid, I. (1990) The influence of microform bed roughness elements on flow and sediment transport in gravel bed rivers. *Earth Surface Processes and Landforms*, 15(8), 739–750. Available from: https://doi.org/10.1002/esp.3290150807

Hassan, M.A., Saletti, M., Johnson, J.P.L., Ferrer-Boix, C., Venditti, J.G. & Church, M. (2020) Experimental insights into the threshold of motion in alluvial channels: sediment supply and streambed state. *Journal of Geophysical Research: Earth Surface*, 125(12), e2020JF005736. Available from: https://doi.org/10.1029/2020JF005736

Hassan, M.A., Saletti, M., Zhang, C., Ferrer-Boix, C., Johnson, J.P.L., Müller, T., et al. (2020) Co-evolution of coarse grain structuring and bed roughness in response to episodic sediment supply in an experimental aggrading channel. *Earth Surface Processes and Landforms*, 45(4), 948–961. Available from: https://doi.org/10.1002/esp.4788

Haynes, H., Vignaga, E. & Holmes, W.M. (2009) Using magnetic resonance imaging for experimental analysis of fine-sediment infiltration into gravel beds. *Sedimentology*, 56(7), 1961–1975. Available from: https://doi.org/10.1111/j.1365-3091.2009.01064.x

Heritage, G.L. & Milan, D.J. (2009) Terrestrial laser scanning of grain roughness in a gravel-bed river. *Geomorphology*, 113(1-2), 4–11. Available from: https://doi.org/10.1016/j.geomorph.2009.03.021

Hilldale, R., Carpenter, W., Goodwiller, B., Chambers, J. & Randle, T. (2015) Installation of impact plates to continuously measure bed load: Elwha River, Washington, USA. *Journal of Hydraulic Engineering*, 141(3), 06014023. Available from: https://doi.org/10.1061/(ASCE)HY.1943-7900.0000975

Hodge, R., Brasington, J. & Richards, K. (2009) In situ characterization of grain-scale fluvial morphology using terrestrial laser scanning. *Earth Surface Processes and Landforms*, 34(7), 954–968. Available from: https://doi.org/10.1002/esp.1780

Hodge, R.A., Hoey, T.B. & Sklar, L.S. (2011) Bedload transport in bedrock rivers: the role of sediment cover in grain entrainment, translation and deposition. *Journal of Geophysical Research - Earth Surface*, 116(F4), F04028. Available from: https://doi.org/10.1029/2011JF002032

Hodge, R.A., Sear, D.A. & Leyland, J. (2013) Spatial variations in surface sediment structure in riffle–pool sequences: a preliminary test of the differential sediment entrainment hypothesis (DSEH). *Earth Surface Processes and Landforms*, 38(5), 449–465. Available from: https://doi.org/10.1002/esp.3290

Hodge, R.A., Voepel, H., Leyland, J., Sear, D.A. & Ahmed, S. (2020) X-ray computed tomography reveals that grain protrusion controls critical shear stress for entrainment of fluvial gravels. *Geology*, 48(2), 149–153. Available from: https://doi.org/10.1130/G46883.1

Hsu, L., Finnegan, N.J. & Brodsky, E.E. (2011) A seismic signature of river bedload transport during storm events. *Geophysical Research Letters*, 38(13), L13407. Available from: https://doi.org/10.1029/2011GL047759

Johnson, J.P.L. (2016) Gravel threshold of motion: a state function of sediment transport disequilibrium? *Earth Surface Dynamics*, 4(3), 685–703. Available from: https://doi.org/10.5194/esurf-4-685-2016

Johnson, J.P.L. (2017) Clustering statistics, roughness feedbacks, and randomness in experimental step-pool morphodynamics. *Geophysical Research Letters*, 44(8), 3653–3662. Available from: https://doi.org/10.1002/2016GL072246

Johnson, M.F., Reid, I., Rice, S.P. & Wood, P.J. (2009) Stabilization of fine gravels by net-spinning caddisfly larvae. *Earth Surface Processes and Landforms*, 34(3), 413–423. Available from: https://doi.org/10.1002/esp.1750

Johnson, M.F., Rice, S.P. & Reid, I. (2011) Increase in coarse sediment transport associated with disturbance of gravel river beds by signal crayfish (Pacifastacus leniusculus). *Earth Surface Processes and Landforms*, 36(12), 1680–1692. Available from: https://doi.org/10.1002/esp.2192

Johnston, C.E., Andrews, E.D. & Pitlick, J. (1998) In situ determination of particle friction angles of fluvial gravels. *Water Resources Research*, 34(8), 2017–2030. Available from: https://doi.org/10.1029/98WR00312

Kalacska, M., Lucanus, O., Sousa, L., Vieira, T. & Arroyo-Mora, J. (2018) Freshwater fish habitat complexity mapping using above and underwater structure-from-motion photogrammetry. *Remote Sensing*, 10(12), 1912. Available from: https://doi.org/10.3390/rs10121912

Kirchner, J.W., Dietrich, W.E., Iseya, F. & Ikeda, H. (1990) The variability of critical shear-stress, friction angle, and grain protrusion in water-

worked sediments. *Sedimentology*, 37(4), 647–672. Available from: https://doi.org/10.1111/j.1365-3091.1990.tb00627.x

Kleinhans, M.G., Jeukens, C.R.L.P.N., Bakker, C.J.G. & Frings, R.M. (2008) Magnetic resonance imaging of coarse sediment. *Sedimentary Geology*, 208(3-4), 69–78. Available from: https://doi.org/10.1016/j.sedgeo.2008.07.002

Lagarde, S., Dietze, M., Gimbert, F., Laronne, J.B., Turowski, J.M. & Halfi, E. (2021) Grain-size distribution and propagation effects on seismic signals generated by bedload transport. *Water Resources Research*, 57(4), e2020WR028700. Available from: https://doi.org/10.1029/2020WR028700

Lakshmanan, S., Pender, G., Haynes, H. & Holmes, W. (2014) Characterization of flow transport within pore spaces of an open-work gravel bed. *International Journal of Engineering & Technology*, 3(4), 457. Available from: https://doi.org/10.14419/ijet.v3i4.3430

Lamb, M.P., Dietrich, W.E. & Venditti, J.G. (2008) Is the critical Shields stress for incipient sediment motion dependent on channel-bed slope? *Journal of Geophysical Research*, 113(F2), F02008. Available from: https://doi.org/10.1029/2007JF000831

Lane, S.N., Tayefi, V., Reid, S.C., Yu, D. & Hardy, R.J. (2007) Interactions between sediment delivery, channel change, climate change and flood risk in a temperate upland environment. *Earth Surface Processes and Landforms*, 32(3), 429–446. Available from: https://doi.org/10.1002/esp.1404

Laronne, J.B. & Carson, M.A. (1976) Interrelationships between bed morphology and bed-material transport for a small, gravel-bed channel. *Sedimentology*, 23(1), 67–85. Available from: https://doi.org/10.1111/j.1365-3091.1976.tb00039.x

Lenzi, M.A., Mao, L. & Comiti, F. (2006) When does bedload transport begin in steep boulder-bed streams? *Hydrological Processes*, 20(16), 3517–3533. Available from: https://doi.org/10.1002/hyp.6168

Lev, E. & Boyce, C.M. (2020) Opportunities for characterizing geological flows using magnetic resonance imaging. *iScience*, 23(9), 101534. Available from: https://doi.org/10.1016/j.isci.2020.101534

Levene, H. (1960) Robust Tests for Equality of Variances. In: *Contributions to probability and statistics: essays in honor of Harold Hotelling*. Palo Alto: Stanford University Press.

Li, Z. & Komar, P.D. (1986) Laboratory measurements of pivoting angles for applications to selective entrainment of gravel in a current. *Sedimentology*, 33(3), 413–423. Available from: https://doi.org/10.1111/j.1365-3091.1986.tb00545.x

Liébault, F., Piégay, H., Cassel, M. & Arnaud, F. (2024) Bedload tracing with RFID tags in gravel-bed rivers: review and meta-analysis after 20 years of field and laboratory experiments. *Earth Surface Processes and Landforms*, 49(1), 147–169. Available from: https://doi.org/10.1002/esp.5704

Lisle, T.E., Nelson, J.M., Pitlick, J., Madej, M.A. & Barkett, B.L. (2000) Variability of bed mobility in natural, gravel-bed channels and adjustments to sediment load at local and reach scales. *Water Resources Research*, 36(12), 3743–3755. Available from: https://doi.org/10.1029/2000WR900238

MacVicar, B.J. & Papangelakis, E. (2022) Lost and found: maximizing the information from a series of bedload tracer surveys. *Earth Surface Processes and Landforms*, 47(2), 399–408. Available from: https://doi.org/10.1002/esp.5255

MacVicar, B.J. & Roy, A.G. (2011) Sediment mobility in a forced riffle-pool. *Geomorphology*, 125(3), 445–456. Available from: https://doi.org/10.1016/j.geomorph.2010.10.031

Madej, M.A., Sutherland, D.G., Lisle, T.E. & Pryor, B. (2009) Channel responses to varying sediment input: a flume experiment modeled after Redwood Creek, California. *Geomorphology*, 103(4), 507–519. Available from: https://doi.org/10.1016/j.geomorph.2008.07.017

Maniatis, G. (2021) On the use of IMU (inertial measurement unit) sensors in geomorphology. *Earth Surface Processes and Landforms*, 46(11), 2136–2140. Available from: https://doi.org/10.1002/esp.5197

Mao, L., Uyttendaele, G., Iroume, A. & Lenzi, M. (2008) Field based analysis of sediment entrainment in two high gradient streams located in Alpine and Andine environments. *Geomorphology*, 93(3-4), 368–383. Available from: https://doi.org/10.1016/j.geomorph.2007.03.008

Marquis, G. & Roy, A. (2012) Using multiple bed load measurements: toward the identification of bed dilation and contraction in gravel-bed rivers. *Journal of Geophysical Research*, 117(F1), 16. Available from: https://doi.org/10.1029/2011JF002120

Masteller, C.C. & Finnegan, N.J. (2017) Interplay between grain protrusion and sediment entrainment in an experimental flume. *Journal of Geophysical Research: Earth Surface*, 122(1), 274–289. Available from: https://doi.org/10.1002/2016JF003943

Masteller, C.C., Finnegan, N.J., Turowski, J.M., Yager, E.M. & Rickenmann, D. (2019) History-dependent threshold for motion revealed by continuous bedload transport measurements in a steep mountain stream. *Geophysical Research Letters*, 46(5), 2583–2591. Available from: https://doi.org/10.1029/2018GL081325

Misset, C., Recking, A., Legout, C., Bakker, M., Bodereau, N., Borgniet, L., et al. (2020) Combining multi-physical measurements to quantify bedload transport and morphodynamics interactions in an Alpine braiding river reach. *Geomorphology*, 351, 106877. Available from: https://doi.org/10.1016/j.geomorph.2019.106877

Monsalve, A., Yager, E.M., Turowski, J.M. & Rickenmann, D. (2016) A probabilistic formulation of bed load transport to include spatial variability of flow and surface grain size distributions. *Water Resources Research*, 52(5), 3579–3598. Available from: https://doi.org/10.1002/2015WR017694

Mueller, E.R., Pitlick, J. & Nelson, J.M. (2005) Variation in the reference shields stress for bed load transport in gravel-bed streams and rivers. *Water Resources Research*, 41(4), W04006. Available from: https://doi.org/10.1029/2004WR003692

Nelson, P.A., Dietrich, W.E. & Venditti, J.G. (2010) Bed topography and the development of forced bed surface patches. *Journal of Geophysical Research*, 115(F4), F04024. Available from: https://doi.org/10.1029/2010JF001747

Nelson, J.M., Shreve, R.L., McLean, S.R. & Drake, T.G. (1995) Role of near-bed turbulence structure in bed load transport and bed form mechanics. *Water Resources Research*, 31(8), 2071–2086. Available from: https://doi.org/10.1029/95WR00976

Nitsche, M., Rickenmann, D., Turowski, J.M., Badoux, A. & Kirchner, J.W. (2011) Evaluation of bedload transport predictions using flow resistance equations to account for macro-roughness in steep mountain streams. *Water Resources Research*, 47(8), W08513. Available from: https://doi.org/10.1029/2011WR010645

Noonan, M.J., Markham, A., Newman, C., Trigoni, N., Buesching, C.D., Ellwood, S.A., et al. (2015) A new magneto-inductive tracking technique to uncover subterranean activity: what do animals do underground? Jones, K. (Ed). *Methods in Ecology and Evolution*, 6(5), 510–520. Available from: https://doi.org/10.1111/2041-210X.12348

Ockelford, A.-M. & Haynes, H. (2013) The impact of stress history on bed structure. *Earth Surface Processes and Landforms*, 38(7), 717–727. Available from: https://doi.org/10.1002/esp.3348

Oldmeadow, D.F. & Church, M. (2006) A field experiment on streambed stabilization by gravel structures. *Geomorphology*, 78(3-4), 335–350. Available from: https://doi.org/10.1016/j.geomorph.2006.02.002

Olinde, L. & Johnson, J.P.L. (2015) Using RFID and accelerometer-embedded tracers to measure probabilities of transport, step lengths, and rest times in a mountain stream. *Water Resources Research*, 51(9), 7572–7589. Available from: https://doi.org/10.1002/2014WR016120

Parker, G. (1990) Surface-based bedload transport relation for gravel rivers. *Journal of Hydraulic Research*, 28(4), 417–436. Available from: https://doi.org/10.1080/00221689009499058

Pearson, E., Smith, M.W., Klaar, M.J. & Brown, L.E. (2017) Can high resolution 3D topographic surveys provide reliable grain size estimates in gravel bed rivers? *Geomorphology*, 293(Part A), 143–155. Available from: https://doi.org/10.1016/j.geomorph.2017.05.015

Penn, A., Tsuji, T., Brunner, D.O., Boyce, C.M., Pruessmann, K.P. & Müller, C.R. (2017) Real-time probing of granular dynamics with magnetic resonance. *Science Advances*, 3(9), e1701879. Available from: https://doi.org/10.1126/sciadv.1701879

Perret, E., Berni, C. & Camenen, B. (2020) How does the bed surface impact low-magnitude bedload transport rates over gravel-bed

rivers? *Earth Surface Processes and Landforms*, 45(5), 1181–1197. Available from: https://doi.org/10.1002/esp.4792

Perret, E., Camenen, B., Berni, C., El Kadi, A.K. & Renard, B. (2023) Uncertainties in models predicting critical bed shear stress of Cohesionless particles. *Journal of Hydraulic Engineering*, 149(4), 04023002. Available from: https://doi.org/10.1061/JHEND8.HYENG-13101

Pfeiffer, A.M., Finnegan, N.J. & Willenbring, J.K. (2017) Sediment supply controls equilibrium channel geometry in gravel rivers. *Proceedings of the National Academy of Sciences*, 201612907(13), 3346–3351. Available from: https://doi.org/10.1073/pnas.1612907114

Phillips, C.B. & Jerolmack, D.J. (2019) Bankfull transport capacity and the threshold of motion in coarse-grained rivers. *Water Resources Research*, 55(12), 11316–11330. Available from: https://doi.org/10.1029/2019WR025455

Phillips, C.B., Masteller, C.C., Slater, L.J., Dunne, K.B.J., Francalanci, S., Lanzoni, S., et al. (2022) Threshold constraints on the size, shape and stability of alluvial rivers. *Nature Reviews Earth and Environment*, 3(6), 406–419. Available from: https://doi.org/10.1038/s43017-022-00282-z

Pledger, A.G., Rice, S.P. & Millett, J. (2014) Reduced bed material stability and increased bedload transport caused by foraging fish: a flume study with juvenile Barbel (Barbus barbus). *Earth Surface Processes and Landforms*, 39(11), 1500–1513. Available from: https://doi.org/10.1002/esp.3592

Polvi, L.E. (2021) Morphodynamics of boulder-bed semi-alluvial streams in northern Fennoscandia: a flume experiment to determine sediment self-organization. *Water Resources Research*, 57(3), e2020WR028859. Available from: https://doi.org/10.1029/2020WR028859

Prancevic, J.P. & Lamb, M.P. (2015) Particle friction angles in steep mountain channels. *Journal of Geophysical Research: Earth Surface*, 120(2), 242–259. Available from: https://doi.org/10.1002/2014JF003286

Pretzlav, K.L.G., Johnson, J.P.L. & Bradley, D.N. (2020) Smartrock transport in a mountain stream: bedload hysteresis and changing thresholds of motion. *Water Resources Research*, 56(11), e2020WR028150. Available from: https://doi.org/10.1029/2020WR028150

Pretzlav, K.L.G., Johnson, J.P.L. & Bradley, D.N. (2021) Smartrock transport from seconds to seasons: shear stress controls on gravel diffusion inferred from hop and rest scaling. *Geophysical Research Letters*, 48(9), e2020GL091991. Available from: https://doi.org/10.1029/2020GL091991

Purinton, B. & Bookhagen, B. (2019) Introducing PebbleCounts: a grain-sizing tool for photo surveys of dynamic gravel-bed rivers. *Earth Surface Dynamics Discussions*, 7, 859–877. Available from: https://doi.org/10.5194/esurf-2019-20

Recking, A. (2009) Theoretical development on the effects of changing flow hydraulics on incipient bed load motion. *Water Resources Research*, 45(4), W04401. Available from: https://doi.org/10.1029/2008WR006826

Recking, A. (2010) A comparison between flume and field bed load transport data and consequences for surface-based bed load transport prediction. *Water Resources Research*, 46(3), W03518. Available from: https://doi.org/10.1029/2009WR008007

Reid, I., Frostick, L. & Layman, J. (1985) The incidence and nature of bedload transport during flood flows in coarse-grained alluvial channels. *Earth Surface Processes and Landforms*, 10(1), 33–44. Available from: https://doi.org/10.1002/esp.3290100107

Reid, I., Layman, J.T. & Frostick, L.E. (1980) The continuous measurement of bedload discharge. *Journal of Hydraulic Research*, 18(3), 243–249. Available from: https://doi.org/10.1080/00221688009499550

Rickenmann, D. (2018) Variability of bed load transport during six summers of continuous measurements in two Austrian Mountain streams (Fischbach and Ruetz). *Water Resources Research*, 54(1), 107–131. Available from: https://doi.org/10.1002/2017WR021376

Rickenmann, D. (2020) Effect of sediment supply on cyclic fluctuations of the disequilibrium ratio and threshold transport discharge, inferred from bedload transport measurements over 27 years at the Swiss Erlenbach stream. *Water Resources Research*, 56(11), e2020WR027741. Available from: https://doi.org/10.1029/2020WR027741

Rickenmann, D., Turowski, J.M., Fritschi, B., Klaiber, A. & Ludwig, A. (2012) Bedload transport measurements at the Erlenbach stream with geophones and automated basket samplers. *Earth Surface Processes and Landforms*, 37(9), 1000–1011. Available from: https://doi.org/10.1002/esp.3225

Robert, A. (1988) Statistical properties of sediment bed profiles in alluvial channels. *Mathematical Geology*, 20(3), 205–225. Available from: https://doi.org/10.1007/BF00890254

Roth, D.L., Finnegan, N.J., Brodsky, E.E., Cook, K.L., Stark, C.P. & Wang, H.W. (2014) Migration of a coarse fluvial sediment pulse detected by hysteresis in bedload generated seismic waves. *Earth and Planetary Science Letters*, 404, 144–153. Available from: https://doi.org/10.1016/j.epsl.2014.07.019

Rychkov, I., Brasington, J. & Vericat, D. (2012) Computational and methodological aspects of terrestrial surface analysis based on point clouds. *Computers & Geosciences*, 42, 64–70. Available from: https://doi.org/10.1016/j.cageo.2012.02.011

Sanders, H., Mason, R.J., Mills, D.N. & Rice, S.P. (2022) Stabilisation of fluvial bed sediments by invasive quagga mussels (*Dreissena bugensis*). *Earth Surface Processes and Landforms*, 47(14), 3259–3275. Available from: https://doi.org/10.1002/esp.5455

Sanguinito, S. & Johnson, J. (2012) Quantifying gravel overlap and dislodgement forces on natural river bars: implications for particle entrainment. *Earth Surface Processes and Landforms*, 37(1), 134–141. Available from: https://doi.org/10.1002/esp.2237

Scheingross, J.S., Winchell, E.W., Lamb, M.P. & Dietrich, W.E. (2013) Influence of bed patchiness, slope, grain hiding, and form drag on gravel mobilization in very steep streams. *Journal of Geophysical Research: Earth Surface*, 118(2), 982–1001. Available from: https://doi.org/10.1002/jgrf.20067

Schmandt, B., Aster, R.C., Scherler, D., Tsai, V.C. & Karlstrom, K. (2013) Multiple fluvial processes detected by riverside seismic and infrasound monitoring of a controlled flood in the Grand Canyon. *Geophysical Research Letters*, 40, 4858–4863. Available from: https://doi.org/10.1002/grl.50953

Schmandt, B., Gaeuman, D., Stewart, R., Hansen, S.M., Tsai, V.C. & Smith, J. (2017) Seismic array constraints on reach-scale bedload transport. *Geology*, 45(4), 299–302. Available from: https://doi.org/10.1130/G38639.1

Schmeeckle, M.W., Nelson, J.M. & Shreve, R.L. (2007) Forces on stationary particles in near-bed turbulent flows. *Journal of Geophysical Research - Earth Surface*, 112(F2), F02003. Available from: https://doi.org/10.1029/2006JF000536

Schneider, J.M., Rickenmann, D., Turowski, J.M. & Kirchner, J.W. (2015) Self-adjustment of stream bed roughness and flow velocity in a steep mountain channel. *Water Resources Research*, 51(10), 7838–7859. Available from: https://doi.org/10.1002/2015WR016934

Sear, D.A. (1996) Sediment transport processes in pool–riffle sequences. *Earth Surface Processes and Landforms*, 21(3), 241–262. Available from: https://doi.org/10.1002/(SICI)1096-9837(199603)21:3<241::AID-ESP623>3.0.CO;2-1

Sear, D.A. (2003) Event bed load yield measurement with load cell bed load traps and prediction of bed load yield from hydrograph shape. In: Bogen, J., Fergus, T. & Walling, D.E. (Eds.) *Erosion and sediment transport measurement in Rivers: technological and methodological advances (proceedings of the Oslo workshop, June 2002)*. Wallingford, UK: IAHS Press, pp. 146–153.

Sear, D.A., Lee, M., Collins, M. & Carling, P.A. (2002) The Intelligent Pebble: A New Technology for Tracking Particle Movements in Fluvial and Littoral Environments. In: *Proceedings of erosion and sediment transport measurement: technological and methodological advances workshop, Oslo, Norway*. Wallingford, UK: IAHS Press, pp. 19–21.

Sederman, A.J., Mantle, M.D., Buckley, C. & Gladden, L.F. (2004) MRI technique for measurement of velocity vectors, acceleration, and autocorrelation functions in turbulent flow. *Journal of Magnetic Resonance*, 166(2), 182–189. Available from: https://doi.org/10.1016/j.jmr.2003.10.016

Segura, C. & Pitlick, J. (2015) Coupling fluvial-hydraulic models to predict gravel transport in spatially variable flows. *Journal of Geophysical*

Research: Earth Surface, 120(5), 834–855. Available from: https://doi.org/10.1002/2014JF003302

Shields, A. (1936) *Anwendung der Aehnlichkeitsmechanik und der Turbulenzforschung auf die Geschiebebewegung*. PhD Thesis Technical. University Berlin.

Smart, G., Aberle, J., Duncan, M. & Walsh, J. (2004) Measurement and analysis of alluvial bed roughness. *Journal of Hydraulic Research*, 42(3), 227–237. Available from: https://doi.org/10.1080/00221686.2004.9641191

Smith, H.E.J., Monsalve, A.D., Turowski, J.M., Rickenmann, D. & Yager, E.M. (2023) Controls of local grain size distribution, bed structure, and flow conditions on sediment mobility. *Earth Surface Processes and Landforms*, 48(10), 1990–2004. Available from: https://doi.org/10.1002/esp.5599

Smith, M., Vericat, D. & Gibbins, C. (2012) Through-water terrestrial laser scanning of gravel beds at the patch scale. *Earth Surface Processes and Landforms*, 37(4), 411–421. Available from: https://doi.org/10.1002/esp.2254

Snyder, N.P., Castele, M.R. & Wright, J.R. (2009) Bedload entrainment in low-gradient paraglacial coastal rivers of Maine, U.S.A.: implications for habitat restoration. *Geomorphology*, 103(3), 430–446. Available from: https://doi.org/10.1016/j.geomorph.2008.07.013

Sokal, R.R. & Rohlf, F.J. (1995) *Biometry: the principles and practice of statistics in biological research*, 3rd edition. New York: W.H. Freeman.

Steer, P., Guerit, L., Lague, D., Crave, A. & Gourdon, A. (2022) Size, shape and orientation matter: fast and semi-automatic measurement of grain geometries from 3D point clouds. *Earth Surface Dynamics*, 10(6), 1211–1232. Available from: https://doi.org/10.5194/esurf-10-1211-2022

Tomsett, C. & Leyland, J. (2019) Remote sensing of river corridors: a review of current trends and future directions. *River Research and Applications*, 35(7), 779–803. Available from: https://doi.org/10.1002/rra.3479

Tsai, V.C., Minchew, B., Lamb, M.P. & Ampuero, J.-P. (2012) A physical model for seismic noise generation from sediment transport in rivers. *Geophysical Research Letters*, 39(2), L02404. Available from: https://doi.org/10.1029/2011GL050255

Turowski, J.M., Badoux, A. & Rickenmann, D. (2011) Start and end of bedload transport in gravel-bed streams. *Geophysical Research Letters*, 38(4), 5. Available from: https://doi.org/10.1029/2010GL046558

Vázquez-Tarrío, D., Borgniet, L., Liébault, F. & Recking, A. (2017) Using UAS optical imagery and SfM photogrammetry to characterize the surface grain size of gravel bars in a braided river (Vénéon River, French Alps). *Geomorphology*, 285, 94–105. Available from: https://doi.org/10.1016/j.geomorph.2017.01.039

Voepel, H., Leyland, J., Hodge, R., Ahmed, S. & Sear, D. (2019) Development of a vector-based 3D grain entrainment model with application to X-ray computed tomography (XCT) scanned riverbed sediment. *Earth Surface Processes and Landforms*, 44(15), 3057–3077. Available from: https://doi.org/10.1002/esp.4608

Warburton, J. & Demir, T. (2000) Influence of bed material shape on sediment transport in gravel-bed rivers: a field experiment. In: Foster, I. (Ed.) *Tracers in geomorphology*. Chichester: John Wiley & Sons, pp. 401–410.

Wiberg, P.L. & Smith, J.D. (1987) Calculations of the critical shear stress for motion of uniform and heterogeneous sediments. *Water Resources Research*, 23(8), 1471–1480. Available from: https://doi.org/10.1029/WR023i008p01471

Wilcock, P.R. & Crowe, J.C. (2003) Surface-based transport model for mixed-size sediment. *Journal of Hydraulic Engineering*, 129(2), 120–128. Available from: https://doi.org/10.1061/(ASCE)0733-9429(2003)129:2(120)

Wittenberg, L. & Newson, M.D. (2005) Particle clusters in gravel-bed rivers: an experimental morphological approach to bed material transport and stability concepts. *Earth Surface Processes and Landforms*, 30(11), 1351–1368. Available from: https://doi.org/10.1002/esp.1184

Woodget, A.S. & Austrums, R. (2017) Subaerial gravel size measurement using topographic data derived from a UAV-SfM approach. *Earth Surface Processes and Landforms*, 42(9), 1434–1443. Available from: https://doi.org/10.1002/esp.4139

Wu, F.-C., Wang, C.-K. & Lo, H.P. (2021) FKgrain: a topography-based software tool for grain segmentation and sizing using factorial kriging. *Earth Science Informatics*, 14(4), 2411–2421. Available from: https://doi.org/10.1007/s12145-021-00660-z

Yager, E.M., Dietrich, W.E., Kirchner, J.W. & McArdell, B.W. (2012) Patch dynamics and stability in steep, rough streams. *Journal of Geophysical Research*, 117(F2), 16. Available from: https://doi.org/10.1029/2011JF002253

Yager, E.M., Kirchner, J.W. & Dietrich, W.E. (2007) Calculating bed load transport in steep boulder bed channels. *Water Resources Research*, 43(7), W07418. Available from: https://doi.org/10.1029/2006WR005432

Yager, E.M., Schmeeckle, M.W. & Badoux, A. (2018) Resistance is not futile: grain resistance controls on observed critical Shields stress variations. *Journal of Geophysical Research: Earth Surface*, 123(12), 3308–3322. Available from: https://doi.org/10.1029/2018JF004817

Yager, E.M., Shim, J., Hodge, R.A., Monsalve, A., Tonina, D. & Johnson, J.P.L. (2024) Automated protrusion, grain size, and critical shear stress estimates from 3D point clouds. *Earth Surface Processes and Landforms*, 1–16.

Yager, E.M., Turowski, J.M., Rickenmann, D. & McArdell, B.W. (2012) Sediment supply, grain protrusion, and bedload transport in mountain streams. *Geophysical Research Letters*, 39(10), L10402. Available from: https://doi.org/10.1029/2012GL051654

Yager, E.M., Venditti, J.G., Smith, H.J. & Schmeeckle, M.W. (2018) The trouble with shear stress. *Geomorphology*, 323, 41–50. Available from: https://doi.org/10.1016/j.geomorph.2018.09.008

Yang, J.Q., Chung, H. & Nepf, H.M. (2016) The onset of sediment transport in vegetated channels predicted by turbulent kinetic energy. *Geophysical Research Letters*, 43(21), 11,261–11,268. Available from: https://doi.org/10.1002/2016GL071092

How to cite this article: Hodge, R.A., Voepel, H.E., Yager, E.M., Leyland, J., Johnson, J.P.L., Sear, D.A. et al. (2024) Improving predictions of critical shear stress in gravel bed rivers: Identifying the onset of sediment transport and quantifying sediment structure. *Earth Surface Processes and Landforms*, 49(8), 2517–2537. Available from: https://doi.org/10.1002/esp.5842